In response to the two reviewer's helpful comments, we have improved the manuscript in various ways. The most major changes to the manuscript:

1. **Language regarding the novelty of the velocity texture method for retrieving echo top height (ETH) has been removed from the abstract and potential advantages of such a methodology are now more explicitly delineated. In addition, we have clarified how we are deriving the ETH.**
2. **Our comparison of the ETHs against the MTSAT data has now been extended to the 2006-2011 timeframe when the VISST version 2 data were available.**
3. **All multipanel figures are now labelled by letter for each panel for easier readability.**
4. **The ETHs were reprocessed to account for cloud layers above the precipitating convection. This resulted in some changes to the conclusions.**
5. **The amount of subpanels in the section analyzing the diurnal cycle have now been reduced for easier readability as some panels did not add to the manuscript.**
6. **We have now more explicitly defined our definition of "congestus" and "deep convection" in a manner that should be both easier to interpret and is consistent with what has been done in past literature.**
7. **We have added an objective analysis of the number of MCSes and also looked at how the convective areas vary in the differing large scale forcing regimes.**
8. **We have more explicitly linked how the differences in the thermodynamic profiles between an active and inactive MJO can contribute to the differences in the ETHs observed between an active and inactive MJO.**

More minor changes to the manuscript are detailed in our response to the reviewers' comments. We again thank the two reviewers for taking the time to provide helpful comments.

Review
: ACP-2018-408
Title: A 17 year climatology of convective cloud top heights in Darwin
Recommendation: Major Revision.
Summary
This study examines the variability of convective echo-top heights (ETH) observed by long-term CPOL radar in Darwin Australia as functions of large-scale conditions during active/suppressed MJO and monsoon/break periods. A new technique to estimate ETH is described and compared to a traditional reflectivity threshold based technique, and to a short period of geostationary satellite retrieved cloud-top heights. The study then continues to partition ETH distributions by combining MJO phases with monsoon indices, and concludes that MJO has relatively stronger influence to convective ETH than monsoon.

In general, I think there are valuable results presented in this paper, particularly illustrating the MJO activity over Australia are relatively more important in regulating convective ETH compared to monsoon vs. break conditions, which previous studies have not investigated. However, there are many aspects of the study that need improvement to make it a significant contribution worthy of publication in ACP.

First, the “novel new technique” described in this study does not prove to be any better (or even different) than simpler existing method in calculating ETH, at least based on the short and in my opinion problematic comparison with a passive satellite cloud-top height retrieval dataset. Then why make a big deal about it? There is nothing wrong with using existing ETH technique, especially if you can’t show that this new method works better than previous ones.

We would like to thank the reviewer for their insightful comments on this manuscript. In a phase randomized radar significant returns have a “Smooth” radial velocity while regions of no return or multi-path have radial velocity that varies randomly from -nyquist to +nyquist. This allows texture of radial velocity to provide a very “clean” determination of a significant return. Most importantly it provides a consistent definition of echo top height rather than relying on an arbitrary threshold. Texture allows the echo top height to match the height of minimum detectable signal.
We have rephrased the “novel new technique” wording in the abstract to simply state that we are assessing the applicability of such a methodology. This therefore reduces the scope of this section from attempting to state which methodology better estimates the cloud top height to simply a comparison that assesses the sensitivity of our results to the ETH retrieval technique used. We still compare the retrieved ETHs against cloud top heights estimated from satellites in order to assess whether or not the retrieval can capture the statistical variability in ETHs without necessarily knowing the uncertainty. Given a dataset as large as this, this approach is feasible as this tells us that we can observe the relative interseasonal variability in ETHs. Furthermore, we feel that it is

important to show the sensitivity of the ETHs to the retrieval technique used, which few studies do, even if a null result is shown.

Given the revision in scope of Section 3, the new wording in the abstract rephases the testing to demonstrate that there is little sensitivity to the ETH with retrieval technique and that our retrieval captures the relative seasonal variability in cloud top height:

"Retrieved ETHs are correlated with those from MTSAT retrieved cloud top heights, showing that the ETHs capture the relative variability in cloud top heights over seasonal scales. "

The wording in Section 3 regarding the methodology comparison already stated that both methods were roughly equivalent, so no changes were made there. However, since both methodologies give similar echo top heights as shown in the comparison in Section 3, we still elect to use the velocity texture methodology since it provides comparable results to using reflectivity.

Second, I think the author need to connect the relative difference in large-scale conditions between active/suppressed MJO and monsoon/break to help explain why MJO has stronger modulation to convective ETH. Looking more at the difference in variability of the sounding profiles (rather than just the mean) between those conditions may be useful.

We have added 5th and 95th percentiles to Figures 4 and 5 to represent the variability seen in each of the large scale forcing regimes and also now add specific humidity. We also now better connect the differences between the large scale forcings in the discussion of Figures 4 and 5 by examining the differences in the distributions of winds and specific humidities, with two paragraphs in Section 3.3 instead of one demonstrating the relative differences between the regimes. In it is shown in this section now that:

1. **There is a greater variability in the Surface to 500 hPa winds during an inactive MJO, which contributes to fewer cases where stronger flow of moisture from the west are occurring.**
2. **There is reduced mid-level moisture (4 to 8 km) during inactive MJO/break conditions, as well as wider variability of such moisture as indicated by the specific humidity profiles. This suggests that the large scale environment during an active MJO is more favorable for the transition of congestus to deep convection.**

Third, the study misses an opportunity to examine how do these different large-scale regimes modulate an important aspect of convection in Darwin: the variability of convective cell sizes. Several recent studies have pointed out the importance of convective cell sizes to mass flux, a critical aspect to cumulus parameterizations. Also, analyses of spatial scales of convection would provide more concrete conclusions on changes

of MCS activities with large-scale regimes, which the paper makes many reference but did not show supporting evidence.

We have added an analysis of both how the cell sizes vary and now objectively quantify the number of MCSes using Rowe and Houze (2014)'s methodology to justify our claims about MCS coverage. In addition we have added material to the introduction now introducing why cell size is important and what past studies have concluded about how the cell sizes in Darwin vary in differing large scale forcings in the introduction. We thank the reviewer for this suggestion!

I provided more detail comments below on various places in the paper that need improvement. Because I do see the value of the long-term tropical radar observations, I recommend major revision of the paper before it can be accepted for publication.

Major Comments

1. Page 2 line 20, please be more specific on what aspects of convective parameterizations are "poor". Poor in doing what?

We have replaced this sentence to be more specific by what we mean by "convective parameterizations are poor:"

Also, convective parameterizations in GCMs do not account for mesoscale organization resulting in insufficient sensitivity to upper tropospheric humidity (Del Genio, 2012).

2. Section 3.1, what kind of quality control procedures were applied to the raw radial radar data? How do you handle ground clutter, AP, and noise that are particularly prevalent in CPOL data at lower level, which could affect your ETH estimates?

The great advantage of the use of velocity texture compared to using reflectivity is that the noise floor can be detected automatically since we expect the velocity field in regions of noise and second trip echoes to be random, resulting in higher velocity textures. We are also doing the following steps:

- **Excluding gates with differential reflectivity < -3 and > 7 dB.**
- **Excluding gates with < 0.45 cross-correlation coefficient.**
- **Excluding gates with differential phase texture > 20**
- **Excluding gates with reflectivity less than -20 dBZ and greater than 80 dBZ.**

We have added these steps into a bulleted list into Section 3.1

3. Page 4 line 18, why choose a "box" when the radar scans are circular? The diagonal

corners of the box are 140 km away from CPOL, which is much further than 100 km radius where sampling and resolution are better.

We chose a "box" since we interpolated the radial data onto a Cartesian grid for easier spatial analysis and using boxes is easier with data in Cartesian coordinates. While creating the Cartesian grid, we used Barnes (1964)'s weighting function with a radius of influence that increases with distance from the radar in order to account for the decreased sampling and resolution as a function of distance from the radar. We conducted visual analyses of such grids and had determined that using a 100 km by 100 km box gave reasonable coverage, even at ranges of 140 km.

4. Page 5 paragraph 2 and 3, I do not understand how is ETH estimated in CPOL using the Doppler velocity standard deviation (σ) technique. Figure 2 shows example of using $\Sigma > 3$ to remove non-precipitating radar echoes, but then how is ETH determined from the remaining echoes? How is it different from simply just using Z threshold > 5 dBZ?

Previously, the ETH was determined by looking at the gate above the highest valid gate after the σ technique was applied. The ETH is now determined by looking for the first echo in the column that is masked using the σ technique. We have added some clarifying wording in this paragraph to explain how we retrieve the ETHs from the masked data: "*The ETHs are then determined by looking at the lowest gate in the column that is masked. We use the lowest gate in the column in order to ensure that we are capturing the ETHs of the precipitating convection, and not that of detrained anvils and cirrus that can lie above the precipitating convection.***"**

This is different from using Z > 5 dBZ as we are not using reflectivity at all.

5. Please also clarify how is ETH estimated using the Z > 5 dBZ threshold method. Do you go from surface upwards and find the first height level where Z drops below 5 dBZ? Or do you go from top downwards to find first level where Z exceeds 5 dBZ (i.e. max height of 5 dBZ in a column)? They could give very different results because the second approach would get cirrus/anvil clouds that are above precipitating convective cloud-tops (particularly for existence of multi-layer clouds).

We had originally used the topmost point in the column where Z > 5 dBZ, or the second approach. However, in order to account for cases of multi-layer clouds, we have switched to the first approach as it is more representative of the precipitating convection. We now also make it more clear how we are deriving the ETH from Z in Section 3.

6. Figure 3, the authors did not provide enough detail about how the CPOL data and MTSAT data are matched for the comparison. Given the two datasets have different spatial resolution, do you match them by interpolating one to another? Do you only compare grid points that both CPOL and MTSAT identified as echo/cloud?

We interpolated the MTSAT data to CPOL's grid and now say so in Section 3.2. In addition we also state that we only compare points that were identified as in cloud by the VISST product and as convective by the Steiner et al. (1995) algorithm in CPOL.

"Since the two datasets are at differing resolution, the MTSAT data are interpolated onto the same grid as the CPOL data for the comparison. Furthermore, to ensure that we are comparing points that are in precipitating convection we both only include points from MTSAT where the VISST product identified cloud and where the convective classification algorithm, detailed in Section 3.4, classified the grid points as precipitating convection."

7. There is also the issue of daytime vs. nighttime retrieval differences in the MT-SAT data. As I mentioned in minor comment 7, there are two satellite retrieval algorithms separately for daytime and nighttime. My previous experience working with these datasets are they do not necessarily provide consistent cloud-top height retrievals when switching from one to another. Cloud-top heights from the same cloud systems can differ as much as several kilometers between the two estimates, and during twilight hours (+/- 1-2 hour) when the solar zenith angle is high, the retrievals uncertainties are very large. Did you 1) compare daytime vs. nighttime separately? 2) exclude twilight hours?

We had not originally done these separations. We went ahead and separated Figure 3c by retrievals made in the daytime and excluded twilight and placed them in the figures below. Our results are insensitive to the time of day.

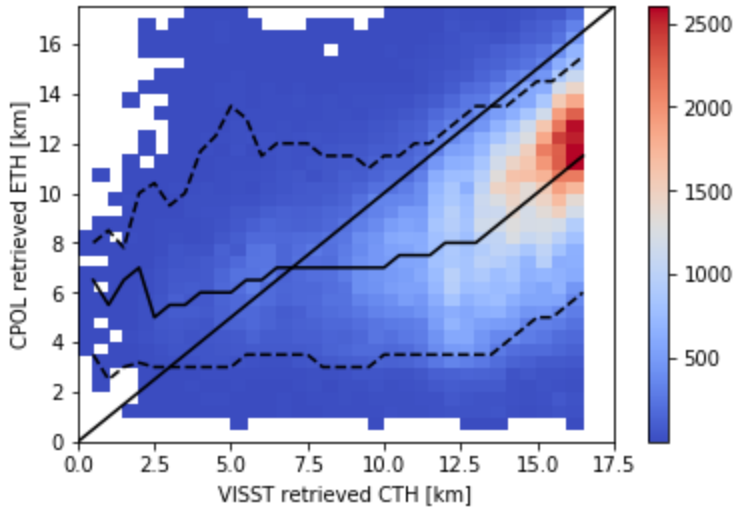

Frequency histogram of VISST retrieved cloud top heights versus CPOL retrieved ETHs using the σ during the daytime (600 to 1700 local time).

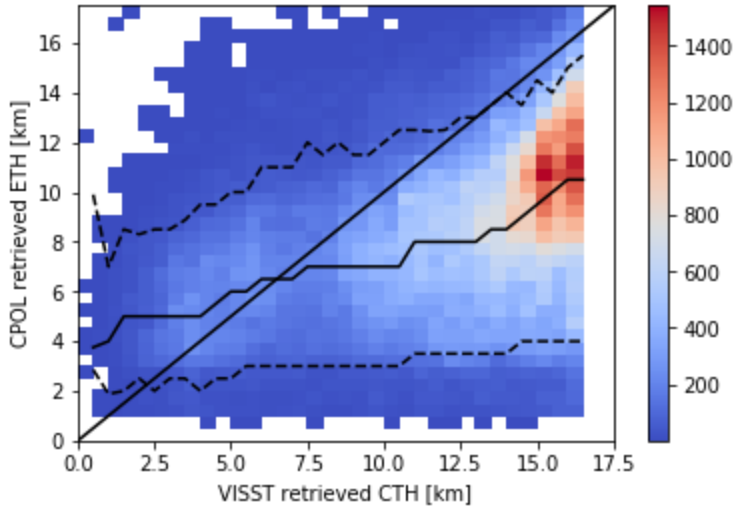

As above, but during night time

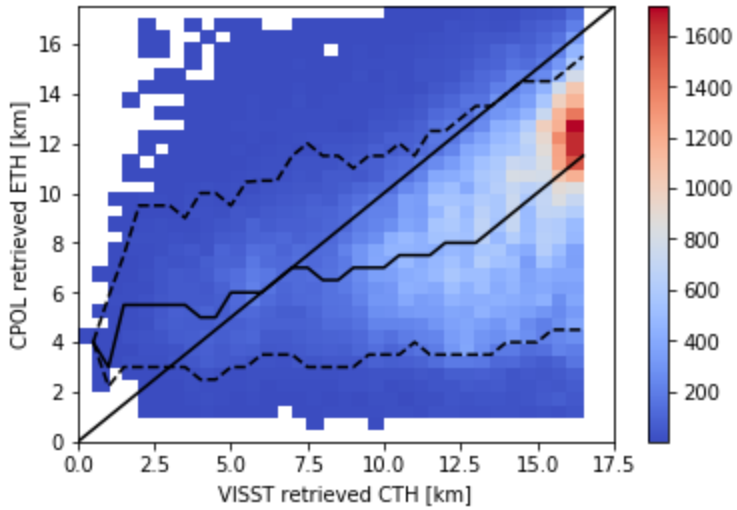

As above, but with twilight hours excluded

8. Why do you choose such a short period of only two months during the peak monsoon TWP-ICE period for a comparison? Particularly when most of the precipitating clouds are deeper than 7-8 km. MTSAT retrievals at this location are available for multiple years in the ARM data archive. Further, wouldn't a more direct comparison be made between CloudSat measured cloud-top heights as it is active remote sensing? For such a long CPOL record and decent spatial coverage, there should be plenty of samples to compare. One of the coauthors of the study (Alain Protat) has made much harder comparisons between CloudSat and ARM cloud radars before (Protat et al. 2014), what stop you from doing that? I understand it takes some effort to do that, but if the paper wants to claim that this new method of estimate ETH from CPOL is closer

to actual cloud-top height, then a more stringent evaluation is needed than what is presented here.

We had chosen the two month period during TWP-ICE because the MTSAT data in the ARM archive initially because we, although now we have extended the comparison from 2006 until 2010 where the version 4 MTSAT data are available. We decided to choose this time period because as same version of the VISST product was available to ensure that differences in processing between the differing versions of the VISST product did not interfere with the comparison. Therefore, we now have done a more comprehensive comparison of the ETHs with those from MTSAT than what was done before.

Using CloudSat data instead of MTSAT data for the comparison provides us with even fewer data points. Figures R1 and R2 show the derived from the CloudSat calculated using the highest point where the echoes are classified as "good" in the Level 2 compared to those derived using Z < 5 dBZ (Figure R1) and $\sigma < 3$. The gate from CloudSat was compared to the nearest grid point in the CPOL data for the comparison. While there is CloudSat data present from the years 2006 to 2017, since the comparisons are limited to the areas scanned by the CloudSat granules, we only have 2,387 datapoints for comparison compared to having . Therefore, the issue of there being relatively few samples also applies to the CloudSat data. Therefore, we elect to use the MTSAT data in the comparison, as there is actually more data in the two month period we analyzed than in all of the CloudSat granules.

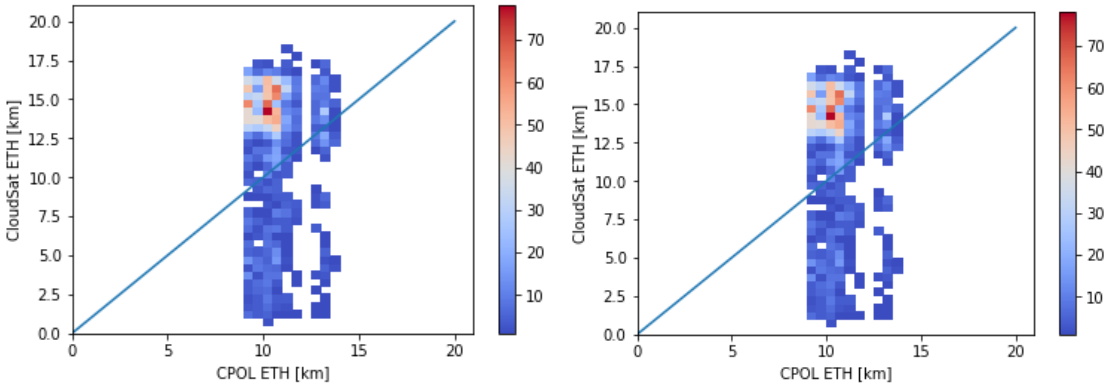

(left) The 2D frequency distribution of ETH derived from CPOL using the highest gate where $\sigma < 3$. compared against ETH derived from CloudSat. (right) as left, but using the highest gate where Z > 5 dBZ.

9. Page 5 lines 26-29, if the new technique using Σ to calculate ETH (which I do not understand, see major comment 4) gives a similar result with a much simpler Z threshold approach, what is so unique about this new approach then if it does not perform better than existing ones? Why make a big deal about the novelty?

This new approach has the major advantage in that, one the noise floor is automatically detected, and, two, second trip echoes are removed. Also, the approach that uses velocity texture is immune to radar miscalibration and therefore can be applied more readily to radar datasets than techniques that use reflectivity. Further, since 5 dBZ can be well above the noise floor of the

In this particular case, we have shown that there is little sensitivity in the retrieved ETHs to whether or not one uses reflectivity or velocity texture. Therefore, we have reframed the comparison as a sensitivity test and removed claims in the paper about the novelty of the approach. Rather, we now claim that our ETH retrieval is robust given how little sensitivity there is.

10. Page 6 line 30, I cannot tell if there is a significant difference in dew point temperature between monsoon break and active period from Fig. 3-4 as they look very similar. You should also compare specific and relative humidity profiles. Mid-level humidity in the tropics is particularly important for supporting deep convection (e.g. Hagos et al. 2014). Showing the difference between the profiles may be useful. Also, given the small difference in the mean thermodynamic profiles between MJO phases, showing a difference in the mean and the variability is useful as well. Please also include the number of soundings that go into the composite.

We thank the reviewer for this very useful comment. We have added specific humidity profiles to Figures 4 and 5 as well as added the amount of soundings that we derived the profiles from in the figure captions. Given concerns from the other reviewer regarding there being too many variables to look at in the paper, we did not add relative humidity to Figures 4 and 5.

The specific humidity at the mid levels is about 1 g/kg higher when the MJO is active and during monsoon conditions. The Hagos et al. (2014) study would suggest that enhanced mid level moisture facilitates the transition from shallow to deep convection, which is consistent with the relative unimodality and the relative unimodality we see in MJO-active/monsoon conditions. Furthermore, the new analysis now shows a greater variability in the winds and specific humidity during MJO inactive/break conditions, which makes for

11. Figure 6, can you comment on why in this study the “overshooting” mode found in Kumar et al. (2013) is not visible in the much longer dataset? Their study showed that the overshooting mode correspond to intense low-level reflectivity (and inferred larger and more numerous raindrop particles), which tend to occur more during the monsoon break period. Does the 14 km peak in break period (Fig. 6 MJO=1,2) correspond to that mode?

With the new processing as suggested by previous comments from this reviewer, the 14 km peak has disappeared. However, we have added discussion on the presence of ETH greater than 15 km, which are only present during break conditions.

12. The congestus mode in Kumar et al. (2013) is defined as ETH < 6.5 km, where in this study it is 8 km. That is not a small difference. 8 km is also significantly higher than the 0C (4.5-5.0 km) level where above which freezing and additional latent heating acceleration of vertical motion can occur. Can you comment on why you choose a larger ETH value for congestus?

We had originally defined the congestus and deep modes corresponding to the μ_1 and μ_2 derived from the bimodal Gaussian fits which resulted in larger values than what is typically considered congestus. In order to be more consistent with the past literature, we still base our classification of congestus and deep convection from the fits, but now place stricter criteria on what is classified as "congestus" versus "deep convective:"

1. **If the ETH distribution is bimodal (0.1 < A < 0.9) then mode 1 is the congestus mode and, mode 2 is the deep convective mode**
2. **If the ETH distribution is unimodal (A < 0.1) and μ_2 < 6.5 km then the single mode is the congestus mode, otherwise the single mode is the deep convective mode**
3. **If the ETH distribution is unimodal (A > 0.9) and μ_1 < 6.5 km then the single mode is the congestus mode, otherwise the single mode is the deep convective mode**

13. Page 8 line 16-18, I thought A is the contribution of mode 1 (congestus), when A increase to 0.9 during active phases of the MJO under monsoon conditions, doesn't that mean most of the convection are congestus, as opposed to deep convection stated in this sentence? That is contrary to the statement of mostly widespread MCSs during active MJO and monsoon. I think the issue here is using only echo-top height to indicate congestus vs. deep convection is too simplistic. The wide spread MCSs are likely associated with much larger but not as deep convective cells compare to more isolated but deep convection during break period. One very important indicator for organized convection, i.e., the size of convective cells is ignored in this study. Larger convective cells and larger updrafts (i.e. in MCSs) carry a majority of the mass flux as reported in both observational analyses (Kumar et al. 2015, Masunaga and Luo 2016) and high-resolution model results (Hagos et al. 2018). The size of convective cells is just as important (if not more) as the depth of the convective cells. It can be easily quantified with the CPOL data and I think would be a useful quantity to investigate as functions of large-scale regimes along with the ETH analyses.

We thank the reviewer for this helpful comment. We have taken care to more carefully define congestus and deep convection in response to this reviewer's major comment number 12. Doing this has improved the presentation of the results in this section and reduces confusion.

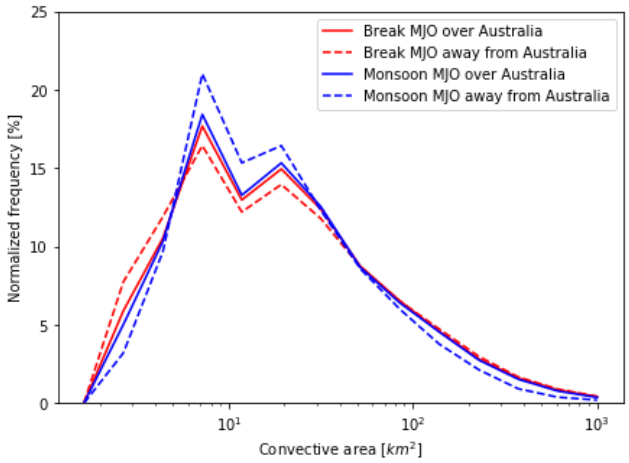

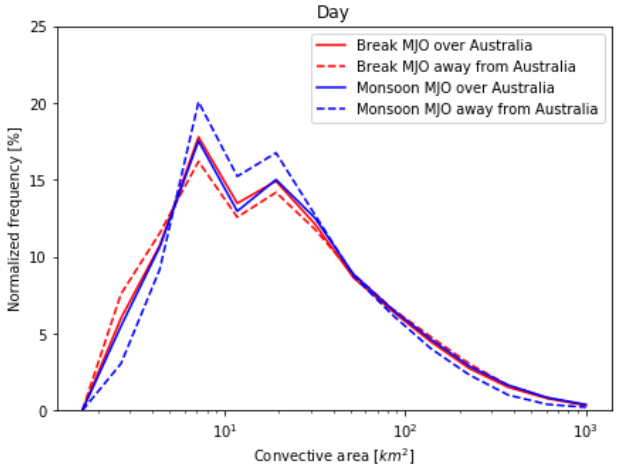

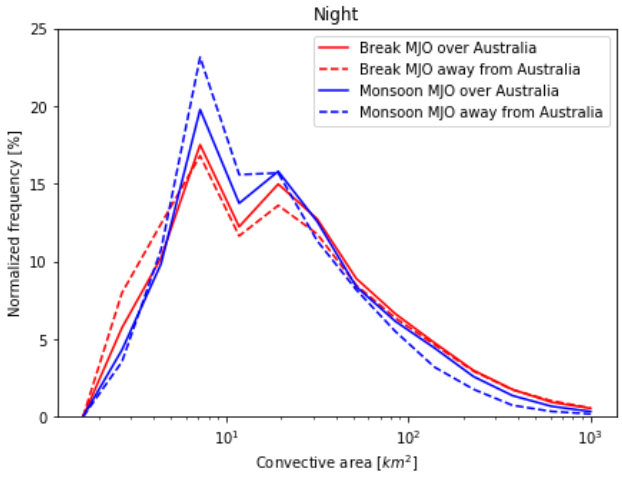

We now discuss the convective areas as a function of large scale forcing, noting that there are generally lower convective areas in monsoon or active MJO conditions, which would be consistent with generally weaker convection being present during these conditions. We use this analysis, in combination with the quantitative MCS analysis

suggested by the reviewer to show that monsoonal conditions are characterized by weaker, but more frequent MCSes.

14. Page 8 line 29-30, I think this is an interesting and important finding. It would be useful to discuss what aspects of the large-scale conditions can help explain larger difference under active MJO (i.e. going back to Fig. 4-5, see major comment 10 about quantifying their relative environment profile difference between active/suppressed MJO, monsoon/break).

Thank you. We have added a couple of sentences of discussion here on how the differences in the environmental profiles observed between MJO phases could be contributing to the differences in the ETHs seen:
"*Considering that, in Figures 4a and 5a show greater increases in equivalent potential temperature with height above the 5 km stable layer during MJO inactive conditions, this suggests that the midlevel thermodynamic profiles support greater inhibition of the convection in the deep convective mode when the active phase of the MJO is away from Australia."*

With the new ETH processing and more careful definition of the modes, we also now observe that the congestus mode is more sensitive to the presence of the monsoon while the deep convective mode is more sensitive to the presence of the MJO

15. Figure 9, other than the more obvious enhanced frequency of deep convective during daytime, the difference for the rest of the panels between MJO phases are difficult to see. Perhaps adding a difference panel would help.

We attempted to add a difference panel to Figure 9, but this made the figure too busy to be readable. Given that the other reviewer commented that there were too many variables in the paper, we did not add a difference panel here.

16. Page 9 line 26-29, why do you have to guess that the enhanced nighttime peak over the ocean during monsoon period is due to MJO? It is relatively easy to identify MCSs in CPOL data (e.g., Rowe et al. 2014 used a simple criteria of precipitation feature major axis length > 100 km to identify MCS in ground-based radar observations), why not actually quantify MCS frequency changes to better support your claim?

We have quantified the radar coverage of MCSes using the methodology of Rowe and Houze (2014) for each scan as the reviewer suggested and have added the average number of MCSes in the radar domain per scan for a given large scale forcing regime and time of day in Table 1. The normalization was done to ensure that differences in the number of MCSes identified was not due to the differing lengths of time spent in each regime.

The results in Table 1 clearly show that, during both an active MJO and active monsoon, that on average more MCSes are present in the radar domain during these conditions. On average, there is also increased presence of MCSes during the daytime compared to night time. Therefore, doing a quantitative analysis suggests that, in most conditions except active monsoon, there are more MCSes at night than during the day. Therefore, most of the conclusions we had before still hold, and where any changes had to be made the discussion was changed accordingly. We also now refer to the frequencies in Table 1 in addition to the already provided references to justify our claims of MCS frequency in Section 4.

17. Figures 10-11, given the strong diurnal cycle between land vs. oceanic area shown in Figures 8-9, did you separate land area and ocean area when calculating their ETH occurrence? I also suggest plotting Figures 10-11 in local time to make it easier for Readers.

We did not initially separate the diurnal cycle figures by land and ocean. At the suggestion of the other reviewer who was concerned about too many variables being presented in this section we have not added an extra figure separating the diurnal cycle by land and ocean.
Figures 10 and 11 are now plotted as a function of local time.

18. Page 11 line 13-14, which figure shows a peak of ETH around 5-6 km during break conditions? Figure 6 when MJO is away from Australia (phases 1-2) generally show a peak between 6-8 km, but drops to 4 km in phases 3-4.

We have modified this conclusion to be more consistent with the analysis in Figure 6, which has changed with the ETH reprocessing.

Minor Comments
1. Page 1 line 2, technically validation of convective processes in GCMs do not "re-quire" such statistics, perhaps it's better to say "could benefit from" such statistics.

We have changed the wording in this sentence to the suggested wording from the reviewer.

2. Page 1 line 5, why does it have to be for a specific model? These observations can be useful for any large-scale model validations.

We were focusing on E3SM as for that model there is an undergoing development to have the model compute results at a 12 km resolution that is high enough such that both MCSes are resolves and the assumptions made in convective parameterizations may not apply. However, since we agree that this is really useful for any GCM, we have changed this sentence to state that this dataset is useful for the validation of convective

processes in any GCM.

3. Page 1 line 22, Jensen et al. (1994) stated the 100 W/m2 is solar forcing, not net radiative forcing, please clarify that in the statement.

We have corrected this statement.

4. Page 2 line 19, "...of of an intense..."

We have removed the extra "of."

5. Page 2 line 27, "...for one wet season in and found..." in what?

We have completed this sentence

6. Page 4 line 1, spell out the acronym "ACRF".

Due to a recent change in the name of the ARM Climate Research Facility (ACRF) to ARM Facility, we have changed this to say "ARM Facility."

7. Page 4 line 4-6, I believe the MTSAT data, at least the inferred channel spatial resolution should be 5 km, not 1 km. Also, the VISST technique uses all available geo-stationary satellite channels, including visible, water vapor, near IR, and IR channels to retrieve cloud properties during day time. For nighttime, a different technique SIST is used for the lack of visible channel.

We now mention that the VISST technique uses these two techniques in this sentence. Also, according to the ARM archive, the resolution is 4 km, which we now mention here.

8. Page 5 line 14, you mentioned "normalized frequency distribution", what is the unit of the shading in Figure 3? The large numbers appears to be just a count, if so it is not normalized frequency.

We have removed the word "normalized" from this sentence.

9. Page 5 line 31, do not use "cloud top height" and ETH interchangeably. You have not established in this study that CPOL ETH is equivalent to cloud top height.

We have changed this phrase to say "echo top height."

10. Figs. 3-4, why is the vertical scale different between the two figures?

The vertical scales are all now the same between Figures 3 and 4.

11. Page 7 line 12, spell out p.d.f. in section headings.

We have corrected this to say "normalized frequency distributions" which is actually what is being plotted.

12. Page 8 line 8, "In 7,..." do you mean in "Eq. (1)"?

We meant to say Figure 7. It says so now.

References for Authors' Response

Barnes, S. L., A technique for maximizing details in numerical weather-map analysis. Journal of Applied Meteorology. 3,4,: 396–409, doi:10.1175/1520-0450(1964)003<0396:ATFMDI>2.0.CO;2, 1964

Del Genio, A.D., Representing the Sensitivity of Convective Cloud Systems to Tropospheric Humidity in General Circulation Models, *Surv. Geophys*, 33: 637. https://doi.org/10.1007/s10712-011-9148-9, 2012.

References

Protat, A., S.A. Young, S.A. McFarlane, T. L'Ecuyer, G.G. Mace, J.M. Comstock, C.N. Long, E. Berry, and J. Delanoë, 2014: Reconciling Ground-Based and Space-Based Estimates of the Frequency of Occurrence and Radiative Effect of Clouds around Darwin, Australia. J. Appl. Meteor. Climatol., 53, 456–478, https://doi.org/10.1175/JAMC-

Kumar, V. V., C. Jakob, A. Protat, C. R. Williams, and P. T. May (2015), characteristics of tropical cumulus clouds from wind profiler observations at Darwin, Australia, J. Atmos. Sci., 72, 1837–1855, doi:10.1175/JAS-D-14-0259.1.

Masunaga, H., and Z. J. Luo (2016), Convective and large scale mass flux profiles over tropical oceans determined from synergistic analysis of a suite of satellite observations, J. Geophys. Res. Atmos., 121, 7958–7974, doi: 10.1002/2016JD024753.

Hagos, S., Z. Feng, K. Landu, and C. N. Long (2014), Advection, moistening, and shallow-to-deep convection transitions during the initiation and propagation of Madden-Julian Oscillation, J. Adv. Model. Earth Syst., 06, doi:10.1002/2014MS000335.

Hagos, S., Feng, Z., Plant, R. S., Houze, R. A., Xiao, H. (2018). A stochastic framework for modeling the population dynamics of convective clouds. Journal of Advances in Modeling Earth Systems, 10. https://doi.org/10.1002/2017MS001214.

Rowe, A. K., and R. A. Houze Jr. (2014), Microphysical characteristics of MJO convection over the Indian Ocean during DYNAMO, J. Geophys. Res. Atmos., 119, 2543–2554, doi: 10.1002/2013JD020799.

General Comments This study aims to define characteristics of monsoon phase (break vs active) within context of MJO phase over Australia for northern AU region. 17 years of radar data are used to increase sample size and develop statically significant results. Overall I think this is an interesting study that shows the impact of MJO phase on cloud top heights for active and inactive periods drawing on precipitation and thermodynamic characteristics to explain the results.

We would like to give thanks to the reviewer for taking the time to provide careful feedback on the manuscript. We agree that the results from the long term dataset presented in the paper are an interesting addition to the literature. In response to another reviewer we have re-proccessed the ETH to be defined as the lowest gate in the column where the velocity texture is greater than 3, when previously it was the highest gate in the column where it was less than 3 (not mentioned in the draft manuscript). We have also excluded data greater than 100 km in range This was done to account for regions where a detached anvil or cirrus cloud layer was above the precipitating convection and helps to ensure that we are only including the precipitation convection in our analysis instead of remnant anvils. Furthermore, it was found that the year 2013 was missing from the ETH database, so now data from the year 2013 are included. Therefore, the updated processing of the ETHs has resulted in some changes to the conclusions of this study.

In response to another reviewer we have also added an analysis of the convective areas and quantified the number of MCSs using the technique used by Rowe and Houze (2014). We felt that now that this paper covers more than just the ETHs, we have changed the title to "*A 17 year climatology of the macrophysical properties of convection in Darwin.*"

My major criticism is that the description is confusing and hard to follow in parts of the statistical analysis (Sec. 4.1) and diurnal cycle (Sec. 4.2) sections

as described in the specific comments below. The confusion is due to 1) combination of too many variables to consider when trying to correlate interpretations stated in the text to results shown in selected figures: active vs inactive monsoon, MJO phase, day vs night, ocean vs land; and 2) the text is not always explicit in terms of which panel of a figure is being used to advance the argument. In consequence, I as the reader, have sometimes come to a different conclusion when interpreting the figures in question compared to the authors. I have also noted these instances below.

We agree that there are quite a few variables that we are stratifying the ETHs and convective areas against and it can be quite overwhelming to the reader. However, the macrophysical properties of convection in Darwin are sensitive to numerous factors including the time of day, the phase of the MJO or the monsoon and even the surface characteristics. We strongly feel that it is important to show how the ETHs can vary as as a function of such characteristics.

Since we are unable to outright eliminate any independent variables from our analysis, we have taken some steps to simplify the presentation of the data to make it easier to interpret:

1. **We now use a more rigorous definition of "congestus" versus "deep convection" that is based off of the threshold used by Kumar et al. (2013), who defined the boundary between congestus and deep convection to be 6.5 km. This, not only being more rigorous and consistent with past literature, also makes the results in Section 4.1 and 4.2 easier to read.**
2. **Every multipanel figure are now labelled by letter and each subpanel is now referred to explicitly.**
3. **The figures showing the ETH distributions as a function of time now just show the frequency distributions with time, reducing the number of figures by 1 and cleaning up clutter. This was done as there was little discussion and few conclusions to be made about how bimodality varies throughout the day.**

Furthermore, the other reviewer requested a quantification of MCSes as well as an an analysis of convective areas in order to more adequately characterize the presence of deep convection than what was done in this manuscript. We have added such analysis to the statistical analysis section.

A more modest critique concerns the spectrum width thresholding technique used to discriminate echo top height as opposed to a minimum reflectivity threshold. On the bright side, the method appears to work reasonably well. However, the end results is that there does not seem to be any real difference in the results when compared to simply applying a minimum reflectivity threshold (which is the traditional approach)
so I am left scratching my head when trying to understand the real advantage of the methodology.

We do not use spectrum width in order to determine the echo top height, but rather, we use the texture of the radial velocity field. This is the standard deviation of the radial velocity of a 3 by 3 gate window surrounding a gate and not the standard deviation of the Doppler spectrum. Radars like CPOL that have a phase that varies randomly from pulse to pulse produce radial velocities that vary randomly gate-to-gate when there is no single scattering returned radiation.

The advantage of such an approach is that (1) the noise floor is automatically detected, (2) we can potentially be able to keep regions in cloud where Z is lower than 5 dBZ, which would be more frequent with 50 km range of CPOL. Finally, this methodology is immune to radar miscalibration and less sensitive to attenuation. This would give us, in theory, more representative of the true cloud top height. While we have removed the "novel" and "new" wording in the abstract, we now more explicitly list these advantages in the introduction and frame the discussion as a sensitivity test. We also have improved the explanation of the velocity texture based ETH retrieval technique so that it is easier to understand both how it works and its potential advantages.

While, for this particular dataset, we arrive at the null conclusion that the ETHs retrieved using the velocity texture methodology and using reflectivity are comparable. We feel that the inclusion of null results in a paper is something that should be done more to guide future research on what methodologies have been tried. This is not done enough in papers in our opinion, and given that this section is short, adding a null result does not significantly lengthen the paper.

Specific Comments 1. P. 4, line 12; please define gate spacing and resolution

We have added the 300 m resolution and gate spacing to this section.

2. P. 5, line 7: What is the spatial resolution of the satellite data? If it's less than radar resolution it's not clear what a relative comparison tells us regarding the performance of the radar-based ETH algorithm.

The spatial resolution of the satellite data at 4 km, so interpolation of the satellite data to the radar's grid was needed.

In response to the other reviewer, we have expanded the analysis in this section to 4 years of MTSAT data from 2006 to 2010, using version 4 of the VISST product. While we acknowledge that the coarser resolution of the satellite introduces uncertainties into the satellite retrieval, over time scales of years the relative seasonal variability in cloud top heights should be captured.

3. P. 5, line 15: similar to previous comment - to understand the differences in cpol vs satellite – what is satellite brightness temp keying off of – what depth of cloud is considered?

The VISST technique uses both the solar and infrared channels at multiple wavelengths to retrieve the cloud properties. According to Cheng et al. (2010), the retrieval is keying off of a height "somewhere

below physical cloud top," but they do not quantify exactly where. We have chosen not to attempt to quantify this since this is extremely difficult to do.

4. P. 5, line 17: cc of 0.49 is not very good
This, while weak, is a statistically significant correlation according to a chi-squared test. The mention of the statistical test has been added to this sentence.

5. P. 5, line 20: this statement assumes the satellite is capturing the variability …

Over timescales of seasons and spatial scales of hundreds of kilometers, we would fully expect this to be the case.

6. Fig. 3 please state in the caption what the color shading represents

We now state that the shading represents the number of counts.

7. P 6. Lines 25-30: In references to Figs 4-5, seems like the big differences are between monsoon phase instead of MJO phase?

For the winds, this is the case. We have noted that there is little difference between the wind speeds between active and inactive MJO conditions.

8. P. 7, line 7 – There are several other older references
that show this behavior: Cifelli and Rutledge 1994 (JAS); 1998 (QJRMS)

We have added these references to this sentence.

9. P. 7, line 27-28: some hint of trade wind layer in MJO=3 for break (Fig. 6)?

We have now changed this sentence to acknowledge that we could be sensing some of the trade wind layer during break conditions, but we ultimately need a radar that is sensitive to cloud particles to characterize it:

"*Also, some evidence of the trade wind mode is visible in Figures 6a-h. However, since the 2 km modes in Johnson et al. (1999) and Kumar et al. (2013) were observed using measurements with a cloud radar that would be more sensitive to liquid cloud droplets than CPOL, more sufficient quantification of this mode would require a radar with a lower minimum discernable signal than CPOL."*

10. P. 8, line 8: This is a minor point but it should be noted that the heights of the different modes that are stated here are approximate. For example, in Fig. 7c the height of mode 2 does not appear to actually reach 15 km
...
We have added the word "approximately" before the quantities in this sentence, and fixed the faulty reference to Figure 7.

11. P. 8, line 12-18: there is some confusion looking
at Fig 7. My read of the red line (A=congestus) in MJO phases 4-7 is
~0.05 – 0.6 for break (Fig 7b) – not 0.8-0.5 as described - and
~0.1-0.4 for monsoon (Fig. 7d) – not > 0.9 as described. Also, the statement on line 14 about unimodality is confusing:

Fig 7b,d show that there is a significant contribution from the congestus mode in break conditions while the MJO is over AU (Fig. 7b, MJO phases 6,7). Similar in monsoon conditions for MJO phase 6 – see Fig 7d. I think the confusion noted above could be avoided by stating more clearly which features in specific figure panels are being referred to.

We have made a more rigorous definition of "congestus" versus "deep" convective modes that makes this section easier to understand. We

determine whether the modes present are congestus or deep convection based on the average location of the modes:

1. **If the ETH distribution is bimodal (0.1 < A < 0.9) then mode 1 is the congestus mode and, mode 2 is the deep convective mode**
2. **If the ETH distribution is unimodal (A < 0.1) and μ_2 < 6.5 km then the single mode is the congestus mode, otherwise the single mode is the deep convective mode**
3. **If the ETH distribution is unimodal (A > 0.9) and μ_1 < 6.5 km then the single mode is the congestus mode, otherwise the single mode is the deep convective mode**

The 6.5 km threshold was chosen based off of Kumar et al. (2013).

We agree, the statement about the unimodality was confusing. We removed it.

12. Fig. 8 – please state in the caption and the figure that this is for break conditions

We have added this information to the caption.

13. P. 9 -please call out panels explicitly in reference to Figs. 8-9

Labels have been added to these panels and now the discussion refers to each relevant panel explicitly.

14. The discussion jumps to Fig 10 before discussing Fig. 9

This is no longer the case.

15. P. 9, line 24: which panel of Fig 10? My read of comparing Fig 10 a and Fig 10b is that during the day there is a higher frequency of deep convection when the MJO is over AU (assume that includes Tiwi islands as well) compared to when MJO is elsewhere.

We have added a reference to Figure 10d.

16. P. 9, 25-26: I don't understand the point about what is being extended in this study vs previous work.

We agree, this sentence was quite confusing. We have rephrased this sentence from:

"*Figure 10d shows a greater frequency of deep convective ETHs over the Tiwi Islands when the MJO is inactive over Australia during the day, which is consistent with increased rainfall over this region.*"

17. P. 10 lines 11-12 – where do the number of days come from?

The number of days comes from the sounding classification in Section 3.3

References:

Chang, F.-L., P. Minnis, J. K. Ayers, M. J. McGill, R. Palikonda, D. A. Spangenberg, W. L. Smith Jr., and C. R. Yost (2010), Evaluation of satellite-based upper troposphere cloud top height retrievals in multilayer cloud conditions during TC4, *J. Geophys. Res.*, 115, D00J05, doi: 10.1029/2009JD013305.

A 17 year climatology of ~~convective cloud top heights~~ the macrophysical properties of convection in Darwin

Robert C. Jackson[1], Scott M. Collis[1], Valentin Louf[2], Alain Protat[3], and Leon Majewski[3]

[1]Argonne National Laboratory, 9700 Cass Ave., Lemont, IL, USA
[2]School of Earth, Atmosphere and Environment, Monash University, Clayton, VIC, Australia
[3]Bureau of Meteorology, 700 Collins St, Docklands VIC 3208, Australia

Correspondence to: Robert Jackson (rjackson@anl.gov)

Abstract.

The validation of convective processes in general circulation models ~~requires~~ (GCMs) could benefit from the use of large datasets that provide long term climatologies of the spatial statistics of convection. To that regard, echo top heights (ETHs)~~retrieved~~ , convective areas, and frequencies of mesoscale convective systems (MCSes) from 17 years of data from C-band POLarization (CPOL) Radar are analyzed in varying phases of the Madden-Julian Oscillation (MJO) and Northern Australian Monsoon in order to provide ample validation statistics for ~~the Department of Energy's next generation Earth Energy Exascale Model. In this paper, ETHs are retrieved using a novel methodology that uses the texture of radial velocity. Comparisons of retrieved ETHs against satellite~~ GCM validation. The ETHs calculated using velocity texture and reflectivity provide similar results, showing the ETHs are insensitive to various techniques that can be used. Retrieved ETHs are correlated with those from MTSAT retrieved cloud top heights~~from the split window technique show that the estimated ETH are correlated with, and, on average, are within 3 km of satellite retrieved~~ , showing that the ETHs capture the relative variability in cloud top heights ~~. Using this technique gives comparable ETHs compared to using a reflectivity threshold.~~ over seasonal scales.

Bimodal distributions of ETH, likely attributable to the cumulus congestus and mature stages of convection, are more commonly observed when the active phase of the MJO is ~~away from Australia~~ over Australia due to greater mid-level moisture during the active phase of the MJO. The presence of a convectively stable layer at around 5 km altitude over Darwin inhibiting convection past this level can explain the position of the modes at around ~~5 to 6 km and 12 to 13~~ 2 to 4 km and 7 to 9 km respectively. The spatial distributions show that Hector, a deep convective system that occurs almost daily during the wet season over the Tiwi Islands, and seabreeze convergence lines are likely more common in break conditions. Oceanic mesoscale ~~convective systems (MCSs) are likely~~ MCSs are more common during the night over Darwin. Convective areas were generally smaller and MCSes more frequent during active monsoon conditions. ~~Unimodal distributions of ETH are more common during monsoon conditions and during an active MJO over Darwin, consistent with the presence of widespread MCSs that are commonly associated with both the MJO and the Northern Australian Monsoon.~~ In general, the MJO is a greater control of the ETHs in the deep convective mode observed over Darwin, with ~~generally both lower and more unimodal~~ higher distributions of ETH when the MJO is active over Darwin.

1 Introduction

Convection in the tropics has an important impact on the global radiative budget. For example, anvil cirrus that are detrained from convection can have a ~~radiative~~ solar forcing on the order of 100 $W\ m^{-2}$ (Jensen et al., 1994). The infrared radiative forcing of these anvil cirrus is highly dependent on the temperature, or height where they are present. Furthermore, convection acts as a vehicle to transport moisture to the tropical tropopause layer (15 km) (TTL) (Dessler, 2002) and therefore can significantly affect the distribution of moisture at the tropopause. Furthermore, the largest convective cells account for a majority of the convective mass flux (Kumar et al., 2015; Masunaga and Luo, 2016; Hagos et al., 2018) This shows that the convective cell size is another important factor for determining vertical moisture transport. Therefore, knowledge on the cloud top heights and cell sizes of such convection is ~~needed to determine~~ useful for determining the impact of deep convection on the global radiative budget and upper tropospheric distribution of moisture~~and provides the~~ . This provides a need for a climatology of ~~cloud top heights~~ such cloud macrophysical properties in the tropics that can be used to validate global climate model (GCM) simulations of convection.

A region in the tropics with continuous observations of ~~cloud top heights~~ the macrophysical properties of clouds provides such a climatology. Such a region is located in Darwin, Australia. Decades of continuous observations have been collected in Darwin, including 17 years of plan position indicator (PPI) scans from the C-band Polarization Radar (CPOL). This region is also ideal for developing such a climatology as the synoptic scale forcing can be objectively determined from both determining information about the Northern Australian Monsoon (Drosdowsky, 1996; Pope et al., 2009a) and about the phase of the MJO (Madden and Julian, 1971; Wheeler and Hendon, 2004), both of which can provide the forcing necessary for convection to develop over the Darwin area. For example, high (20-30 dBZ) reflectivities above the freezing level, slightly smaller cells, and greater amounts of lightning have been observed during break convection while monsoonal convection tends to be shallower, more widespread, and less electrically active (Rutledge et al., 1992; Williams et al., 1992; May and Ballinger, 2007; Kumar et al., 2013a, b). Also, the monsoon preferentially onsets when the convectively active phase of the MJO approaches Darwin (Evans et al., 2014), so the MJO and the monsoon are not necessarily independent of each other. Besides convection associated with the MJO and the monsoon, the convection that occurs in this region can also be influenced by the seabreeze and Tiwi Islands, such as the nearly daily summer occurrence of ~~of~~ an intense deep convective system called Hector (Keenan et al., 1989; Crook, 2001). ~~Given the~~ The MJO is poorly resolved in many general circulation models (GCMs) (Gu et al., 2011)~~, and that~~ . Also, convective parameterizations in GCMs ~~are poor~~do not account for mesoscale organization resulting in insufficient sensitivity to upper tropospheric humidity (Del Genio, 2012). Therefore, statistical analyses of how the cloud tops vary for differing phases of the MJO and monsoon are useful for GCM validation~~of convective processes in models such as the Department of Energy's Energy Earth Exascale Model (E3SM)~~.

Past studies have examined the cloud top heights in convection over Darwin and the maritime continent estimated by radar through the echo top height (ETH). Observations in Indonesia by Johnson et al. (1999) showed 3 modes in ETH in convection

during the Tropical Ocean - Global Atmosphere Coupled Ocean Atmospheric Response experiment that corresponded to stable layers: a mode at 2 km, a mode at around 5 km, and a mode at around the tropopause of 15 km. Over Darwin, May and Ballinger (2007) examined the distribution of ETHs in convection for one wet season in and found limited evidence of multimodal distributions of ETH, but had only considered the maximum cloud top height over a cell's lifetime. Furthermore, they found that cloud top heights in break convection were higher than those in monsoonal convection. Kumar et al. (2013b) analyzed two wet seasons of CPOL data and found evidence of bimodal ETH distributions. They also found that convection formed during active monsoon conditions has lower cloud top heights than convection formed during break conditions similar to May and Ballinger (2007). Kumar et al. (2013a) investigated 3 wet seasons of CPOL data in Darwin and found four differing modes that corresponded to trade wind cumulus, cumulus congestus, deep convection and overshooting convection. Therefore, differing conclusions have been reached on the number of modes of convection that are present over Darwin and the maritime continent.

This study improves upon past studies looking at cloud top heights in Darwin in various ways. First, the analysis is expanded to the full CPOL record of 17 wet seasons to ~~perform the analysis~~ analyze the relationship between convective properties and the large-scale environment on a more statistically representative dataset than has been done in Johnson et al. (1999); May and Ballinger (2007); Kumar et al. (2013a, b). This is possible using recent advances in supercomputing and recent developments of highly customizable distributed data analysis packages written in Python such as Dask (Dask Development Team, 2016). Secondly, none of the past studies have looked at how ETHs can vary for differing phases of the MJO. Rauniyar and Walsh (2016) have found that rainfall rates in Darwin are correlated to the presence of the convective phase of the MJO over Darwin. Also, Evans et al. (2014) have observed that the preferential onset of the monsoon is when the active phase of the MJO approaches Australia. Therefore it is worth exploring the possibility that cloud top heights of convection in Darwin are also influenced by the MJO. In this study we wish to answer the following questions:

1. Does the MJO have an influence on the observed convective cloud top heights over the Darwin area?
2. Do the conclusions of past studies regarding the heights of break and monsoonal convection over Darwin ~~extend to~~ still hold when using 17 wet seasons?
3. What are the spatial distributions and diurnal cycles of convective cloud top heights over Darwin during the differing phases of the MJO and monsoon?
4. When do we observe multiple modes in the distributions of cloud top heights when looking at 17 years worth of data?

It is also important to note that ~~these~~ the past studies have used a reflectivity (Z) threshold to determine the ETH~~, which can underestimate the cloud top height since this criteria would filter out regions of cloud without precipitation that are still detectable by CPOL . Therefore,~~ . Using a reflectivity threshold, there is the potential that regions near cloud top that are detected by CPOL could be excluded. Reflectivity fields from CPOL are also prone to miscalibration and attenuation, although these effects have been corrected for as best as possible in the dataset used in what follows. As an independent assessment of these corrections and for sake of comparison of two ETH retrieval techniques, this study also ~~demonstrates~~ assesses the applicability of ~~a new~~ an alternate algorithm that uses velocity texture σ~~to~~, a quantity not affected by radar miscalibration and less likely to be affected by attenuation than Z, to derive the ETH. ~~Finally, an uncertainty analysis is performed where ETHs~~

~~are compared against satellite retrieved cloud top heights in order to quantify the uncertainty in the radar estimated cloud top heights and to assess the~~ This technique also allows for automatic detection of the noise floor of the radar and potentially the inclusion of more regions near cloud top. The feasibility of using ~~the velocity texture technique~~this methodology is assessed by comparing ETHs derived using varying thresholds of σ as well as as Z against satellite retrieved cloud top heights.

The remainder of the paper is organized as follows. Section 2 will go into detail about the data products that are used. Section 3 describes the algorithms used to process the radar data, estimate echo top height, and quantify the synoptic scale forcing over Darwin. Section 4 shows results on how the ETHs vary in differing phases of the MJO, differing monsoonal regimes. Section 4 also shows the diurnal cycle of ETHs over Darwin over varying regions and in various phases of the MJO and monsoon in order to link the ETHs to both large scale and localized mechanisms. Section 5 shows the primary conclusions of this study.

2 Data products

2.1 CPOL

The C-band Polarization (CPOL) radar, located at the Tropical Western Pacific (TWP) Atmospheric Radiation Measurement site in Darwin, Australia (Keenan et al., 1998), conducted Plan Position Indicator (PPI) scans every 10 minutes at 15 elevations ranging from 0.5° to 40° with a 300 m resolution and gate spacing during the summer seasons of 1998 to 2017, excluding 2007 and 2008. While CPOL records polarimetric variables, the variables of interest from CPOL for retrieving ETH are the reflectivity Z and the radial velocity v_r. Other instrumentation was used to supplement information provided by CPOL. Rawinsonde launches were conducted four times per day from the ARM ~~ACRF~~ Facility TWP site, providing vertical profiles of temperature T, dew point T_d, relative humidity RH, and the zonal (u) and meridional (v) components of the wind velocity. In order to estimate the uncertainty in the retrieved ETHs from CPOL, we compare the ETHs against satellite retrieved cloud top heights. To do this, we use the Japanese Multi-functional Transport Satellites (MTSAT) which images brightness temperature T_b every hour at a ~~1~~ 4 km resolution, giving information on cloud top heights estimated by the ~~split window technique (Ohkawara, 2004)~~Visible Infrared Solar Split Technique during the day and the Infrared Solar Split Technique during the night (Minnis et al., 2011). The MTSAT are integrated into the VISST data product version 4 (Minnis et al., 2011) providing cloud top height over a 12° by 12° region centered over Darwin.

3 Data processing algorithms

3.1 Radar data processing

The previous section gave information about the radars and other instruments used in this study. This section details how the echo top heights were estimated from CPOL and evaluated against satellite measurements. The Python ARM Radar Toolkit (Py-ART) (Helmus and Collis, 2016) was used in order to process, grid, and display v_r and Z. Before the velocity texture was calculated, gates that met any of the following criteria were removed in order to remove ground clutter and noise:

1. Z <-20 dBZ or Z > 80 dBZ
2. differential reflectivity > 7 dB or < -3 dB
3. Texture of differential phase greater than 20°
4. Cross-correlation coefficient < 0.45

The velocity texture was then calculated using the standard deviation of the 3 x 3 window surrounding a gate and then was gridded onto a Cartesian grid at a 1 km horizontal and 0.5 km vertical resolution using Barnes (1964)'s interpolation technique. Since at higher elevations and ranges some gaps in the interpolated radar field may be present due to lack of radar sampling at a given location, a radius of influence that increases as a function of distance from the radar was used in order to minimize artifacts generated by radar sampling. Due to the increasing beam width as a function of distance from the radar as well as decreased vertical resolution with height, there is greater uncertainty in the the ETH as distance increases from the radar. Therefore, only data on a 200 by 200 km box surrounding CPOL was used, following (Kumar et al., 2013b) and data less than 20 km from the radar was excluded as the radar does not scan at heights of 20 km at these distances. We use Dask (Dask Development Team, 2016), a package written in Python to analyze datasets on distributed clusters, to map the problem of analyzing the 17 years of CPOL data to the Bebop cluster at Argonne National Laboratory.

3.2 Calculation of ETHs

Now that the radar data has been processed and interpolated onto a Cartesian grid, the next step is to calculate the ETH from CPOL. Past studies (May and Ballinger, 2007; Kumar et al., 2013a, b) have used the highest pixel in the column with Z > 5 dBZ as the ETH, while only including time periods where there were echoes present in all pixels from 2.5 km to the highest pixel with Z > 5 dBZ to remove time periods with a cloud layer above the precipitating convection. Since this threshold can be at least 2 dB above the minimum detectable signal at a range within 100 km of CPOL as seen in Figure 1, using reflectivity (Z) could potentially remove regions that are both detected by CPOL and in cloud, especially for clouds with heights < 10 km and ranges < 60 km from CPOL. Also, Z is prone to errors from both miscalibration and attenuation in heavy rain. Therefore, we examine the possibility in this study of using Doppler velocity texture σ as a threshold instead of Z~~.~~, which is immune from errors from miscalibration and less prone to errors from attenuation than Z.

Figure 2 shows and example of how σ is interpreted. To demonstrate that higher values of σ correspond to noise, Figs. 2a,b show an example field of Z and σ from CPOL for a case of isolated convection on 05 March 2006. Figure 2b shows isolated regions of $\sigma < 3$, corresponding to the regions of precipitation that are seen in Figure 2b. The more widespread regions of $\sigma > 3$ correspond to clutter, noise, and multi-trip echoes that are present in Fig. 2a. ~~Furthermore, when a~~ This is due to the fact, that, in a phase randomized radar such as CPOL, regions of significant returns will have smoother velocity fields and regions of noise will have more random velocity fields, allowing for the automatic detection of the minimum detectable signal. When a threshold of $\sigma > 3$ is used to mask gates in Fig. 2a, Fig. 2c shows that only regions of precipitation are still present after masking~~. Therefore, using σ as a threshold is reasonable for removing regions of noise~~, showing that noise is removed. The

ETHs are then determined by looking at the lowest gate in the column that is masked. We use the lowest gate in the column in order to ensure that we are capturing the ETHs of the precipitating convection, and not that of detrained anvils and cirrus that can lie above the precipitating convection.

However, even despite using a methodology that automatically determines the minimum detectable signal using σ that is immune to radar miscalibration and less prone to errors from attenuation, there is still the possibility that the smallest cloud water droplets ~~and ice crystals with maximum dimensions below about 0.5 mm~~ near cloud top are not detected by CPOL. ~~Furthermore, some regions of precipitation were removed in Figure 2c since a few gates with precipitation have higher σ.~~ Therefore, it is important to assess quantitatively whether the ETHs calculated using the σ threshold represent the variability in cloud top heights that is observed in convection in Darwin and to test the sensitivity of the retrieved ETHs to the retrieval technique used. To do this, ETHs from CPOL are compared against cloud top heights retrieved by MTSAT which provide an independent estimate of cloud top height. Since the MTSAT data are at an hourly temporal resolution, only CPOL scans that were within 10 minutes of a MTSAT record were compared against the MTSAT retrieved cloud top heights ~~for the months of January and February 2006.~~ from March 2006 until December 2010. This time period was chosen as it is the time period covered by Version 4 of the VISST product over Darwin and ensures that the same data processing techniques were used throughout the dataset. Since the two datasets are at differing resolutions, the MTSAT data are interpolated onto the same grid as the CPOL data for the comparison. Furthermore, to ensure that we are comparing points that are in precipitating convection we both only include points from MTSAT where the VISST product identified cloud and where the convective classification algorithm, detailed in Section 3.4, classified the grid points as convection.

Figure 3 shows the results of such comparisons using ~~both the Z threshold of >~~ the lowest gate in the column where $Z < 5$ dBZ, with the 5 dBZ threshold from May and Ballinger (2007) and Kumar et al. (2013a) (Figure 3a)~~and~~. Figures 3bcd use varying thresholds of σ for the ETHs. In all panels of Figure 3, there is considerable spread in the comparison between the satellite cloud top heights and the ETHs retrieved by CPOL. ~~However, there is~~ Time periods within two hours of sunrise and sunset were excluded in the generation of Figure 3 since large uncertainties can exist in the VISST retrieval during twilight hours. Since VISST uses two different retrieval algorithms for day and night time, this can potentially introduce large uncertainties in the retrieved cloud top heights from MTSAT. However, when the data were stratified by day or night time, there was little difference in the generation of Figure 3 (not shown). The coarser resolution of the MTSAT data compared to the CPOL data indicates that smaller scale heterogeneity may not be captured by MTSAT. Nevertheless, it is expected that, over time scales of years and spatial scales of 100 km, the MTSAT captures the interseasonal variability in cloud top height.

There is a clear peak in the ~~normalized~~ frequency distribution present in all panels at ETHs > 7.5 km and the median ETH is within ~~3~~ 4 km of the VISST retrieved cloud top height for ETHs > 2.5 km. Furthermore, the average ETH retrieved from CPOL increases with increasing MTSAT retrieved cloud top height in Figure 3, showing that the ETHs retrieved from CPOL are correlated (Pearson correlation coefficient of 0.49, $p < 0.01$ according to a χ^2-test) with the satellite retrieved cloud top heights. As cloud top heights retrieved by MTSAT can have an uncertainty as high as 3 km (Hamada and Nishi, 2010), it is not possible to determine whether the MTSAT retrieved cloud top heights or CPOL ETHs provide the better estimate of cloud top height. Nevertheless, the correlation between the CPOL ETHs and satellite retrieved cloud top heights shows that the CPOL

retrieved ETHs using ~~σ threshold captures the~~ any of the tested techniques capture the statistical variability in cloud top heights that are observed in Darwin.

~~In Figure 3a, when the May and Ballinger (2007) methodology is used to determine ETH the results are similar to Figure 3c and d, showing that, whether Z or σ are used to retrieve ETH, similar conclusions can be drawn. However, when using a threshold of σ = 2, the spread is greater in Figure 3b, as shown by the increased difference in the 95th and 5th percentiles in Figure 3b compared to the other thresholds, indicating a reduced correlation between ETH and MTSAT-retrieved cloud top height compared to using the other thresholds to calculate ETH.~~ The mean, and ~~5th and 95~~ fifth and ninety-fifth percentiles are similar in Figure 3~~acd~~abcd, showing that there is little difference between using May and Ballinger (2007) and Kumar et al. (2013a)'s technique compared to using σ for calculating ETH. Therefore, there is little sensitivity of the retrieved ETH to the technique used, showing the robustness of the ETH retrieval. Therefore, this study uses the ~~highest gate~~ lowest gate in the column where σ ~~<~~>~~>~~ 3 to be defined as the ETH~~, as there is little difference in the estimates of cloud top heights between using Z and using σ~~.

3.3 Quantification of large scale forcing

Now that a methodology has been developed to ~~estimate the cloud~~ calculate the echo top height from the CPOL data, the next step in this study is to develop methodologies for quantifying the large scale forcing in the Darwin region. The large scale forcing in the Darwin region can be quantified with respect to two major synoptic phenomena. One of them is the Northern Australian Monsoon (Drosdowsky, 1996; Pope et al., 2009a). Its presence is characterized by deep westerly winds over Darwin that provide moisture flow from the Indian Ocean to the Darwin region. Many algorithms have been used in the literature to determine the presence of the Northern Australian Monsoon. However, only Drosdowsky (1996) and Pope et al. (2009a) robustly identify the presence of the monsoon. These algorithms depend on the profile of the zonal component u and meridional component v of the wind as well as temperature, dew point, and pressure collected by rawinsondes over Darwin. The first, Drosdowsky (1996), uses the deep-layer (Surface-500 hPa) mean u in order to characterize the presence of the monsoon. Under this classification, a deep layer of westerly winds is characteristic of the monsoon, which provides an environment where moisture is flowing from the Indian Ocean to Darwin. The second, Pope et al. (2009a), uses k-means clustering on the winds, temperature, and dew point to find five regimes that correspond to differing synoptic scale phenomena in Darwin: deep west, moist east, east, dry east, and shallow west. The "deep west" and "shallow west" regimes corresponds to westerly flow from the surface to 500 hPa, or the active monsoon. The "moist east" regime corresponds to (Drosdowsky, 1996)'s "break" regime where continental convection is more likely to occur, and the other regimes correspond to either suppressed or transitional regimes.

The large scale forcing can also be quantified by the phase of the Madden-Julian Oscillation (Madden and Julian, 1971). The phase of the MJO is quantified using a number 1 to 8 that gives an indicator of the position of the enhanced and suppressed convective activity associated with the MJO. When the MJO phase increases from 1 to 3, the enhanced convective activity is traveling to the east from the Indian Ocean. When the MJO index increases from 4 to 7, the enhanced convective activity is over the maritime continent and traveling east to the Pacific Ocean. When the MJO index is 8, the enhanced convective activity

is over the Pacific Ocean. This MJO index is determined using Wheeler and Hendon (2004)'s database that is based on both the outgoing long-wave radiation from satellites and the 850 to 200 hPa u from reanalysis data. Rauniyar and Walsh (2016) found that the yearly occurrence of the Pope et al. (2009a) regimes has a high amount of interannual variability as they are modulated by the El Nino-Southern Oscillation (ENSO) while the occurrence of the MJO does not. Therefore, the use of Pope et al. (2009a) is less suitable for a sample size of 17 seasons than the use of the MJO for analyzing such a dataset. Furthermore, the five classifications provide more opportunity for over-classification than using Drosdowsky (1996). Therefore, to quantify the large scale forcing over Darwin, the dataset is separated using only the MJO index and the Drosdowsky (1996) monsoon classification. To even further prevent the possibility of over-classification, much of the data in this study are classified into whether the convective phase of the MJO is over Australia (MJO indicies 4 to 7), or when it is not (MJO indicies 1 to 3, 8).

Figures 4 and 5 show the mean thermodynamic and wind profiles for given phases of the MJO and monsoon. ~~Fig. 4shows~~ Figs. 4ef show that break conditions are generally characterized by a layer of east-northeasterly winds extending to about 10 km when the MJO is over Australia and throughout the troposphere when the convective mode of the MJO is elsewhere, while westerlies are prevalent at altitudes up to 8 km during monsoon conditions. ~~This, and the profiles of temperature and dew point point to greater advection of~~ Figure 4cd shows lower fifth percentiles of dewpoint and specific humidity at 4 to 8 km than Figure 5cd, demonstrating a greater number of cases with drier midlevels during break conditions. This is suggestive of conditions that would support deep convection would be less prevalent during active break conditions than during the monsoon (Hagos et al., 2013).

There is a greater variability in the winds below 6 km when the active phase of the MJO is over Australia in Figures 4ef and 5ef. In particular, the 95th percentiles of u are greater below 6 km when the MJO is active over Australia than when the active phase of the MJO is away from Australia in in Figures 4e and 5e. This shows that there are a greater number of cases with westerly flow advecting moisture from the Indian Ocean ~~to Darwin during monsoonal conditions and drier air from Australiain break conditions~~ when the MJO is active over Australia. Furthermore, the difference between the ninety-fifth and fifth percentiles of dewpoint and specific humidity at 4 to 8 km are greater when the active phase of the MJO is away from Australia, as seen in Figs. 4cd and 5cd, showing more variability in mid-level moisture when the MJO is inactive over Australia. Furthermore, mean specific humidities are 0.5 to 2 kg higher when the MJO is active over Australia, as seen in Figures 4d and 5d. Therefore, conditions are expected to be consistently more favorable for supporting deep convection during the active phase of the MJO (Hagos et al., 2013).

The thermodynamic profiles in Figures 4~~and 5~~ a and 5a then show a transition from convectively unstable conditions from ~~the surface~~ 1 km until 4 km to stable at around 4-6 km, or temperatures around $0°C$ with the tropopause located at around 15 km. Three stable layers over Indonesia were observed by Johnson et al. (1999): a trade wind layer at 2 km, a stable layer at around 6 km, and the tropopause at 15 km. This suggests that, while the trade wind stable layer is not present over Darwin, the stable layer at around around $0°C$ that is present over Indonesia is also present over Darwin. The presence of such a layer suggests that any parcel lifted from the surface would easily rise to heights to around 4-6 km, or $0°C$ but would need to be dynamically energetic enough to penetrate through the stable layer above this level. Furthermore, since the stable layer is located at temperatures just below $0°C$, this inhibits the formation of ice which releases latent heat that would invigorate the updraft, further inhibiting

convection. Therefore, an updraft strong enough to reach levels where ice formation to occur would be more likely able to penetrate up to the tropopause. This notion is supported by the observations of vertical velocities in convection that reaches the tropopause typically being strongest above 5 km ~~(May and Rajopadhyaya, 1999; Collis et al., 2013; Varble et al., 2014)~~ (Cifelli and Rutledge, 1994, 1998; May and Rajopadhyaya, 1999; Collis et al., 2013; Varble et al., 2014). This therefore indicates that the thermodynamic profiles favor the formation of two distinct populations of convection: weaker cumulus congestus that do not penetrate heights much past the stable layer and stronger deep convection that would more than likely be able to penetrate the tropopause.

3.4 Quantification of convective areas and MCSes

In addition to the ETH, two other macrophysical properties of the convective systems sampled by CPOL were derived in this study. One, the convective area, was calculated by taking the total area of continuous regions in each scan that were identified as convective by the algorithm of Steiner et al. (1995). This algorithm defines regions with $Z > 40$ dBZ as well as examines the peakedness of the Z field in order to classify regions as convective. This algorithm was designed for convection in the Tropics, and a visual analysis of the algorithm showed that it reasonably distinguished between stratiform and convective regions (not shown). The number of MCSes per radar scan was also determined. This was done by using the methodology previously used by Rowe and Houze (2014), Nesbitt et al. (2006), and others which first defines precipitation features (PFs) as all continuous regions where $Z > 15$ dBZ. After that, the minimum size ellipse that fits around the PF is calculated using the algorithm in Bradski (2000). MCSes are then identified as any ellipses that have a major axis length of greater than 100 km. The number of MCSes were then normalized by the number of scans that were identified to be in the large scale forcing regimes in Section 3.3 and the calculations placed into Table 1. This was done in order to account for the differences in the amount of time spent in each large scale forcing regime over the study period.

4 Statistical analysis/discussion

4.1 ~~p.d.f.s~~ Normalized frequency distributions of ETH and convective area

The previous section detailed the methods and uncertainties in the derived ETHs and gave a meteorological overview of the differing synoptic scale regimes. In this section, the entire 17 year record of ETHs in differing synoptic scale regimes is analyzed in order to provide a climatology of convective cloud top heights. In this analysis, only convective regions are considered, using the Steiner et al. (1995) ~~to define convective regions which uses both a threshold of $Z > 40$ dBZ as well as the peakedness of the Z field in order to classify regions as convective . This algorithm was designed for convection in the Tropics, and a visual analysis of the algorithm showed that it reasonably distinguished between stratiform and convective regions(not shown)~~as mentioned in Section 3.4 to define convective regions.

Figure 6 shows the ~~p.d.f.s~~ normalized frequency distributions of ETHs in differing MJO indicies and monsoonal classifications. Some of the distributions shown in Figure 6 are bimodal with one mode at an ETH of approximately 4 to 8 km and the

other at about 9 to 13 km. The normalized frequency distributions in Figures 6efg provide the best examples of such bimodal normalized frequency distributions. Two of the modes are therefore similar to the largest two modes observed by Johnson et al. (1999): a mode at approximately 4 to 6 km corresponding to the cumulus congestus stage and a mode at ~~15~~ 8 to 10 km corresponding to deep convection. Kumar et al. (2013a) observed 4 modes, with the trade wind cumulus mode at 2 km, congestus mode at heights of 3-6.5 km, deep convection mode at 6.5 to 15 km, and overshooting convection at heights greater than 15 km. Some evidence of overshooting convection is present in 6, particularly during break conditions in 6a-h. Also, some evidence of the trade wind mode is visible in Figures 6a-h. However, since the 2 km modes in Johnson et al. (1999); Kumar et al. (2013a) were observed using measurements with a cloud radar that would be more sensitive to liquid cloud droplets than CPOL, ~~and that there is no inversion at 2 km in Figs. 4, 5, it is not surprising that their trade wind cumulus mode is not observed here~~more sufficient quantification of this mode would require a radar with a lower minimum discernable signal than CPOL.

Therefore, we generally observed bimodal distributions of ETH. May and Ballinger (2007) observed limited evidence of ~~such~~ bimodality, but bimodal distributions of ETH were also found by Kumar et al. (2013b), corresponding to similar heights. The thermodynamic profiles shown in the previous section can explain the bimodality seen in Figure 6. In particular, the presence of a stable layer at heights above 5 km can explain the bimodality seen in some of the regimes in Figure 6. As convection develops and evolves into deeper convection, it will first have to grow to the height of the start of the stable layer and will stop growing in vertical extent there if there is not enough buoyancy to penetrate past it. Updrafts would have to be energetic enough to penetrate the cap, and such updrafts would more than likely penetrate up to the tropopause.

In order to quantify the locations and contributions of the peaks in each p.d.f in Figure 6, bimodal Gaussian fits of the form in Equation (1)

$$P(x) = A\frac{1}{\sigma_1\sqrt{2\pi}}e^{-(x-\mu_1)^2/2\sigma_1^2} + (1-A)\frac{1}{\sigma_2\sqrt{2\pi}}e^{-(x-\mu_2)^2/2\sigma_2^2} \quad (1)$$

where A is the contribution of mode 1, μ_1, μ_2 are the mean and σ_1 and σ_2 are the standard deviations of modes 1 and 2 respectively were generated for each regime~~and plotted onto Figure 7~~. Mode 1 is the mode with smaller ETHs and mode 2 is the mode with larger ETHs. In Figure 7, μ_1 ranges between ~~4 and 8~~ approximately 2 and 6 km and μ_2 ranges between ~~9 and 15 km~~ approximately 7 and 10 km when the distributions are bimodal ($0.1 < A < 0.9$). This shows that~~the~~ , when the distributions are bimodal, the location mode 1 roughly corresponds to the location of the cumulus congestus mode observed by Johnson et al. (1999); Kumar et al. (2013b), and the location of mode 2 corresponding to their deep convective mode but μ_1 was sometimes greater than 6.5, when A was less than 0.1, indicating a unimodal distribution that corresponds to Kumar et al. (2013b)'s deep convective mode. Therefore, in order to properly identify what types of clouds were present, thresholds based on the bimodality and the locations of the modes are required. Therefore, for the rest of this paper, we define the congestus and deep convective modes as follows:

1. If the ETH distribution is bimodal ($0.1 < A < 0.9$) then mode 1 ~~will be referred to as the cumulus~~ is the congestus mode and, mode 2 is the deep convective mode ~~.~~

2. If the ETH distribution is unimodal (A < 0.1) and μ_2 < 6.5 km then the single mode is the congestus mode, otherwise the single mode is the deep convective mode.

3. If the ETH distribution is unimodal (A > 0.9) and μ_1 < 6.5 km then the single mode is the congestus mode, otherwise the single mode is the deep convective mode.

The 6.5 km threshold was chosen following the threshold between congestus and deep convection used by Kumar et al. (2013b) . The μ_1, μ_2, and A from this classification were then plotted onto Figure 7.

The ~~locations~~ contributions of the two modes in Figures 6 and 7 vary with MJO index. As the active phase of the MJO is over Australia (MJO indicies 4 to 7), ~~values of A range from 0.8~~ in Figure 7b the contribution of the congestus and deep convective modes are 40 to ~~0.5 while they are 0.3 to 0.5 in break conditions when the active phase of the MJO is away from Australia. The relative unimodality around ETH of 10 to 12 km present when the active phase of the MJO is over Australia suggests that the MJO contributes to an enhanced presence of deep convection, with less such convection~~ 60% indicating bimodal distributions. However, the frequency distributions are less bimodal when the active phase of the MJO is away from Australia ~~. In~~ as shown in Figures 7b,d. In active monsoon conditions, ~~values of A are greater than 0.65,and greater than 0.9~~ more unimodal distributions with lower ETHs are observed as shown in 7b,d when the active phase of the MJO is ~~over Australia. This indicates that most of the convection observed during both an active monsoonand active MJO are categorized as deep convection. The presence of mostly deep convection during an active MJO and monsoon is also consistent with an increased presence of widespread mesoscale convective systems (MCSs). Indeed, Virts and Houze (2015) have observed an increased number of MCSes in the tropics during the~~ away from Australia. The enhanced mid-level specific humidities during active monsoon/MJO phases in Figures 4d and 5d provide an environment that supports the transition of congestus to deep convection and is likely contributing to the enhanced bimodality of ETHs observed when the active phase of the MJO ~~, and Pope et al. (2009b) have observed an increased number of MCSes over northern Australia during active monsoon conditions, which provides further evidence to support this claim~~is over Australia (Hagos et al., 2013).

The locations of these modes also vary depending on whether or not the active phase of the MJO is present over Australia. In Figure 7a, on average the cumulus congestus mode is located at ~~5.4 (6.6~~ approximately 3.0 (2.8 km) when the MJO is active (inactive) over Australia during break conditions in Figure 7a. During monsoon conditions Figure 7b, this mode is on average at ~~5.5 km (7.6~~ approximately 4.4 km (6.2 km) when the MJO is active (inactive) over Australia. The average locations of the deep convective mode during break conditions ~~become 11.6 and 12.5~~ are approximately 8.1 and 7.9 km during active and inactive MJO conditions respectively. For the monsoon, the average locations are ~~9.5 km and 12.5~~ approximately 8.9 km and 7.5 km during active and inactive MJO conditions respectively. ~~Therefore, on average, convection is penetrating to higher heights both~~ However, a greater percentage of the ETHs are greater than 14 km in Figure 7a than in Fig. 7c, showing that more overshooting tops are present during break conditions~~and~~ . Therefore, on average, when the MJO is ~~inactive over Australia . However, the~~ active over Australia with more overshooting tops present during break conditions.

The change in heights of the deep convective mode associated with an active MJO over Australia is greater than that associated with the monsoon~~. The higher cloud top heights observed during break conditions are consistent the studies of~~

~~May and Ballinger (2007) and Kumar et al. (2013a) who also noted higher cloud top heights in break convection compared to monsoonal convection, but did not examine how convective cloud top heights varied as a function of MJO index.~~ , while congestus are more sensitive to the presence of the monsoon. Considering that, in Figures 4a and 5a show greater increases in equivalent potential temperature with height above the 5 km stable layer during MJO inactive conditions, this suggests that the midlevel thermodynamic profiles support greater inhibition of the convection in the deep convective mode when the active phase of the MJO is away from Australia. Furthermore, Figures 4cd and 5cd showed enhanced mid-level moisture when the MJO was active over Australia which creates an environment more favorable for supporting deep convection (Hagos et al., 2013) . Evans et al. (2014) noted that the monsoon over Darwin will preferentially onset at MJO indicies 3 and 4, so ~~this suggests that the observations of lower convective cloud top heights during an active monsoon as observed May and Ballinger (2007) and Kumar et al. (2013a) could also be attributable to the active phase of the MJO. Therefore~~ that also suggests that future studies that examine the properties of convection in Darwin in differing large scale conditions must also consider the phase of the MJO in addition to the monsoon, as the MJO has been shown here to be of importance.

The convective area is another important indicator of organized convection, as larger convective areas are typically associated with stronger updrafts and more organized convection. Therefore, the normalized frequency distribution of the convective areas are also plotted in Figure 8 for differing phases of the MJO, monsoon, and time of day. During the day, we see similar distributions of convective area between break and active monsoon conditions in 8a when the MJO is active over Australia. However, when the active phase of the MJO is away from Australia, the normalized frequency distribution narrows in active monsoon conditions, showing a fewer cells with areas greater than 100 km^2 and more cells with areas in between 7 and 20 km^2. At night, the difference in the distribution of convective areas between break and monsoon conditions in Figure 8b is greater than that in Figure 8a, with broader distributions of convective areas during break conditions. In general, little trend in the normalized frequency distribution is seen with changing MJO index in Figure 8 This is indicative of stronger updrafts during break conditions compared to monsoon conditions, especially at night. While there is more widespread coverage of MCSes during active monsoon and when the active phase of the MJO is over Australia as indicated in Table 1, the analysis in Figure 8 shows that the lower convective areas observed in active monsoon conditions indicate weaker, but more frequent MCSes. Meanwhile, the fewer MCSes observed, larger cell areas, and the increased presence of overshooting tops in Figure 7a shows that less widespread, but stronger convection is present during break conditions. This is consistent with what has been observed in studies such as Rutledge et al. (1992), Williams et al. (1992), May and Rajopadhyaya (1999), and May and Ballinger (2007) .

4.2 Diurnal cycle and spatial distribution of ETHs

The previous section established that the MJO is a significant control of the ETHs observed over Darwin. However, the mechanisms by which convection over Darwin can be generated can not only depend on the large scale forcing but can also be influenced by localized mechanisms such as seabreezes. Therefore, to investigate under what conditions the formation of convection via localized mechanisms is more likely, Figures ~~?? and ??~~ 9 and 10 show normalized frequencies of occurrence of ETHs > 7 and < 7 km for the given synoptic scale forcing shown in Figures 4 and 5 as a function of space and time. The

threshold of 7 km is shown as it is, on average, the local minimum between the cumulus congestus and deep convective modes in Figure 6. ~~Figure ?? shows~~ Figures 9ab show that, in break conditions, the cumulus congestus are confined to Tiwi islands and the Australian continent during the day and more confined to the ocean at night in Figure 9ef. When the MJO is active over Australia, greater counts are present over the ocean during the day in Figure 9a compared to b than when the active phase is away from Australia. Similar conclusions can be made for deep convection during break conditions in ~~Figure ??~~Figures 9cdgh.

The peak in deep convection isolated over the Tiwi islands present during the day in Figure ~~??~~ 9abcd is a deep convective system that forms almost daily during the wet season called Hector the Convector (Keenan et al., 1989; Crook, 2001). It is likely forced by seabreeze convergence lines and further intensified by cold pools that formed from neighboring cumulus congestus (Dauhut et al., 2016). Given this, in break conditions, both surface level easterly flow onto the Tiwi Islands providing a seabreeze and the presence of cumulus congestus over the Tiwi Islands in Figure ~~??~~ 9ab show that the environment is favorable for Hector to occur. The reduced widespread cloud cover that is observed during break conditions (May et al., 2012) as well as MCS coverage (Table 1 also provides an environment more favorable for localized seabreezes to develop around the Tiwi Islands, and hence for Hector to form. A maximum in rainfall over the Tiwi Islands, attributed to Hector, when the MJO is inactive over Australia has been noted by Rauniyar and Walsh (2016). ~~While Figure ??~~ Figure 9d shows a greater frequency of deep convective ETHs over the Tiwi Islands when the MJO is inactive over Australia during the day, ~~this study extends this conclusion to suggest that Hector is also more active during the day and when the MJO is inactive over Australia~~which is consistent with increased rainfall over this region. During the night, both congestus and deep convection are more focused towards the oceans and the northern Australian coast in Figure ~~??. Given that an~~ 9efgh. An overnight peak in rainfall in the tropics has been attributed to the presence of long lived oceanic MCSs by Nesbitt and Zipser (2003)~~, and that it is very common for MCSs over Darwin to last over 4 hours (Pope et al., 2009b), this is likely the result of such long lived MCSs~~. The data in Table 1 suggests that there is a greater coverage of MCSes during the night in break conditions, consistent with more widespread coverage of overnight MCSes. Kumar et al. (2013a) showed a peak in ETHs over the ocean in the early morning hours and over the coast and continents during the afternoon, so this study extends their conclusion to 17 wet seasons of data.

In active monsoon conditions, cumulus congestus are widespread throughout the western half of the ~~region~~ regionin Figure 10a,e while the deeper convection is mostly focused on the Australian coast in Figure ~~??~~10ce. Fewer occurrences of deep convection on the Tiwi islands are present in in Figure 10cd compared to break conditions, suggesting that conditions are less favorable for the formation of Hector during an active monsoon. Since westerly winds at the surface to 500 hPa are prevalent during an active monsoon, the seabreeze is mostly likely to occur over the western coast of the Tiwi islands and the western Australian coast over Darwin and therefore any seabreeze convergence lines that do form would form there. However, as active monsoon conditions are typically characterized by widespread stratiform cloud cover (May et al., 2012), and there are a greater number of MCSes in active monsoon conditions (Table 1), it is less likely that diurnal solar heating would be as important during an active monsoon. The reduced solar heating during an active monsoon is likely resulting in the reduced occurrences of Hector, as the lack of solar heating decreases the likelihood that localized seabreezes form.

At night, both congestus and deep convection decrease in occurrence on the continents as one goes east in Figures 10e-h. This suggests that oceanic MCSs, common during an active monsoon ~~(May et al., 2012)~~as suggested by May et al. (2012) and

Table 1, are decaying as they approach land from the west as would be expected with the deep westerly flow. During the night they would encounter a drier airmass than over the ocean, causing a depletion of moisture and hence decay. Figure ?? 10 also shows more sporadic occurrences of both congestus and deep convection convective clouds when the MJO is inactive over Australia (Figures 10f,h) compared to when it is active (Figures 10e,g). There are 63 days where the MJO was both inactive over Australia and where an active monsoon occurs, while there are 54 days where the monsoon and MJO are both active over Australia. Meanwhile, 7.9×10^5 occurrences of ETH > 7 km are present when the MJO is inactive and 2.5×10^6 are when the MJO is active in Figure ??10. Therefore, the more sporadic occurrences are not due to the fact that the monsoon and MJO were active for fewer days, but rather this suggests that, even in the presence of deep westerlies that are characteristic of the monsoon, convection is suppressed when the MJO is inactive over Australia. Indeed, Evans et al. (2014) have found that the onset of the monsoon preferentially starts when the MJO indicies are 3 and 4 and decays when MJO indicies are 7 and 8 as the convective phase travels east over the maritime continent. Therefore, it is not surprising to see fewer occurrences of convection when the MJO is inactive over Australia.

To demonstrate how the locations of the modes and total occurrences vary with time of day, Figure ?? 5 shows how the two modes of convection vary as a function of time of day with fits generated from Equation (1) at 2 hour intervals. Figure ?? shows 5a-d show that total counts start to increase at around 400 UTC 1700 local as convection initiates during the late morning hours and transitions from congestus to deep convection. At sunsetmidnight, a decrease in the total number of counts is seen, suggesting that the loss of solar heating, an important factor during break conditions (May et al., 2012), is contributing to the decay of convection. The total counts and then show a second peak during the overnight hours with generally in Figure 5ac with bimodal distributions. This secondary peak during the overnight hours, given the oceanic nature of the overnight convection as suggested by Figures ??, ??, 9e-h, and 10e-h are likely due to nocturnal MCSs that are common over the tropical oceanic regions (Nesbitt and Zipser, 2003). In Figure ??, the ETH distributions are generally bimodal throughout the day when the active an increase in the number of MCSes at night during break conditions as indicated in Table 1. Figures 5bd show the overnight peak is less pronounced when the convective phase of the MJO is away from Australia, and the overnight peak is less pronounced in these conditions. Since MCSs are larger in extent in the convectively active phase of the MJO (Virts and Houze, 2015)as seen by (Virts and Houze, 2015) and more frequent as seen in Table 1, the reduced coverage frequency of MCSs in the inactive phase of the MJO likely explains the decreased contribution of deep convection and hence the bimodality seenin Table 1. Rather, as suggested by the spatial analysis and Rauniyar and Walsh (2016), Hector and seabreeze convergence lines are more likely contributing to the distributions seen here. During monsoon conditions, Figure ?? 5c shows that a majority of the counts occur when the convective phase of the MJO is over Australia and during the daytime hours where the highest frequency of MCSes were identified. Similar conclusions about the peaks of convective activity and bimodality seen in Figure ?? seen in Figs. 5ab can be made in Figure ??Figs. 5c. However, more unimodal distributions of ETH are seen in Figure 5d with little congestus present and few occurrences at night.

5 Conclusions

~~Radar estimated~~ This study examined the macrophysical properties of convection in Darwin in differing phases of the MJO and Northern Australian Monsoon, including the echo top heights~~from convection that was present~~ , convective areas, and number of mesoscale convective systems detected by CPOL during 17 wet seasons~~was scanned by the C-band Polarization Radar (CPOL)~~ . The ETHs were generated using a ~~velocity-texture based methodology . This methodology differed~~ methodology that uses velocity texture, differing from past studies that used reflectivity based thresholds such as May and Ballinger (2007); Kumar et al. (2013a, b). The use of velocity texture provides the potential for an automatic detection of the noise floor which increases the capability of including the lowest reflectivties that still correspond to meteorological echoes and is also immune to radar miscalibration. It is demonstrated that such ~~a methodology is reasonable to use for estimating the echo top height as they~~ ETHs are correlated with cloud top heights retrieved by ~~brightness temperatures from satellites (Ohkawara, 2004; Minnis et al., 2011) . This comparison also demonstrates the null result when comparing the ETHs against those retrieved by a reflectivity threshold: the ETHs generated using thresholds based off of velocity texture and reflectivity are similar for convection sampled by CPOL.~~

satellites (Ohkawara, 2004; Minnis et al., 2011) and that there is little sensitivity to ETH to whether reflectivity or velocity texture is used to retrieve the ETH, showing that retrievals of ETH are robust. These echo top heights, along with convective areas and the occurrences of MCSes, are then sorted by the Wheeler and Hendon (2004) MJO index and Drosdowsky (1996) monsoon/break classification. Some key conclusions can be made from this data:

1. Bimodal echo top heights were observed, and more common during break conditions, with a peak at around ~~5 to 6~~ 3 to 4 km and another around ~~10 to 12~~ 7 to 9 km, likely corresponding to cumulus congestus and deep convection. The break between these peaks corresponds with the presence of a stable layer at 5 km inhibiting the development of more intermediate convection.

2. Unimodal distributions were more common during an active ~~MJO and an active~~ monsoon, with ~~mostly deep convection~~ an enhanced level of MCSes being observed during these periods as indicated by an increased average number of MCSes present. This is consistent with past studies suggesting that long lived MCSes are present during these conditions. ~~In general the~~ The lower convective areas observed in active monsoon conditions, especially at night, indicate that these MCSes are generally weaker than those observed during break conditions. The MJO is a more important control of cloud top heights of deep convection than the phase of the monsoon for the 17 years of data shown here, with lower echo top heights observed when the MJO is ~~active over Australia.~~ away from Australia. For the ETHs of congestus, we show that the monsoon is a greater control of the observed ETHs.

3. The observed cloud top heights during the day in break and MJO-inactive conditions showed the presence of Hector and cumulus congestus. Meanwhile, at night, the distributions of echo top heights ~~showing mostly deep convection combined with the general characteristics of convection observed during the MJO and active monsoon are more consistent with the presence of widespread long lived MCSes during~~ along with the analysis of the ~~night time hours~~ number of MCSes observed showed that oceanic MCSes were more prevalent during the nighttime hours during break and MJO-inactive conditions.

4. The fewest occurrences of convection were observed during both an inactive MJO and an inactive monsoon. Given that there were more days observed during an inactive MJO and inactive monsoon than when the MJO and monsoon were active over Australia, this shows that convection is suppressed during these conditions.

The observed distributions of echo top heights and convective areas seen here create a suitable climatology for the validation of convective parameterizations in global climate models and are in the process of being used for the validation of the ~~DOE's E3SM~~ Department of Energy's Energy Exascale Earth System Model model. Future studies should focus on the improvement of the representation of the MJO and the monsoon in global climate models, as these results demonstrate the clear importance of both phenomena in determining the properties of convection observed in Northern Australia. It is also clear from the research presented here that the MJO is important for determining the properties of convection over Darwin and future studies looking at aspects of convection such as vertical velocities ~~and convective area~~ should consider the influence of the MJO as well as the monsoon.

Code availability. The code used to generate these plots is available at https://github.com/EVS-ATMOS/cmdv-rrm-anl/. The code used to generate velocity texture is included in the Python Atmospheric Radiation Measurement (ARM) Radar toolkit, available at http://github.com/ARM-DOE/pyart

Data availability. The data used to generate the cloud top height dataset is in the process of being submitted to the Atmospheric Radiation Measurement (ARM) Archive and will be available as a PI product upon publication of this manuscript.

Competing interests. There are no competing interests for this manuscript.

Acknowledgements. Argonne National Laboratory's work was supported by the U.S. Department of Energy, Office of Science, Office of Biological and Environmental Research, under Contract DE-AC02-06CH11357. This work has been supported by the Office of Biological and Environmental Research (OBER) of the U.S. Department of Energy (DOE) as part of the Climate Model Development and Validation activity. The development of the Python ARM radar toolkit, was funded by the ARM program part of the Office of Biological and Environmental Research (OBER) of the U.S. Department of Energy (DOE). The work Monash University and the Bureau of Meteorology was partly supported by the U.S. Department of Energy Atmospheric Systems Research Program through the grant DE-SC0014063. We gratefully acknowledge use of the Bebop cluster in the Laboratory Computing Resource Center at Argonne National Laboratory. The bulk of the code has been written using the open-source NumPy, Scipy, Matplotlib, Jupyter and Dask projects, and the authors are grateful to the authors of these projects. Special thanks are given to Brad Atkinson and Dennis Klau for the continual upkeep of the CPOL radar.

References

Barnes, S. L.: A Technique for Maximizing Details in Numerical Weather Map Analysis, Journal of Applied Meteorology, 3, 396–409, https://doi.org/10.1175/1520-0450(1964)003<0396:ATFMDI>2.0.CO;2, https://doi.org/10.1175/1520-0450(1964)003<0396:ATFMDI>2.0.CO;2, 1964.

Bradski, G.: The OpenCV Library, Dr. Dobb's Journal of Software Tools, 2000.

Cifelli, R. and Rutledge, S. A.: Vertical Motion Structure in Maritime continent mesoscale Convective Systems: Results from a 50-MHz Profiler, Journal of the Atmospheric Sciences, 51, 2631–2652, https://doi.org/10.1175/1520-0469(1994)051<2631:VMSIMC>2.0.CO;2, https://doi.org/10.1175/1520-0469(1994)051<2631:VMSIMC>2.0.CO;2, 1994.

Cifelli, R. and Rutledge, S. A.: Vertical motion, diabatic heating, and rainfall characteristics in north Australia convective systems, Quarterly Journal of the Royal Meteorological Society, 124, 1133–1162, https://doi.org/10.1002/qj.49712454806, https://rmets.onlinelibrary.wiley.com/doi/abs/10.1002/qj.49712454806, 1998.

Collis, S., Protat, A., May, P. T., and Williams, C.: Statistics of Storm Updraft Velocities from TWP-ICE Including Verification with Profiling Measurements, Journal of Applied Meteorology and Climatology, 52, 1909–1922, https://doi.org/10.1175/JAMC-D-12-0230.1, https://doi.org/10.1175/JAMC-D-12-0230.1, 2013.

Crook, N. A.: Understanding Hector: The Dynamics of Island Thunderstorms, Monthly Weather Review, 129, 1550–1563, https://doi.org/10.1175/1520-0493(2001)129<1550:UHTDOI>2.0.CO;2, https://doi.org/10.1175/1520-0493(2001)129<1550:UHTDOI>2.0.CO;2, 2001.

Dask Development Team: Dask: Library for dynamic task scheduling, http://dask.pydata.org, 2016.

Dauhut, T., Chaboureau, J.-P., Escobar, J., and Mascart, P.: Giga-LES of Hector the Convector and Its Two Tallest Updrafts up to the Stratosphere, Journal of the Atmospheric Sciences, 73, 5041–5060, https://doi.org/10.1175/JAS-D-16-0083.1, https://doi.org/10.1175/JAS-D-16-0083.1, 2016.

Del Genio, A. D.: Representing the Sensitivity of Convective Cloud Systems to Tropospheric Humidity in General Circulation Models, Surveys in Geophysics, 33, 637–656, https://doi.org/10.1007/s10712-011-9148-9, https://doi.org/10.1007/s10712-011-9148-9, 2012.

Dessler, A. E.: The effect of deep, tropical convection on the tropical tropopause layer, Journal of Geophysical Research: Atmospheres, 107, ACH 6–1–ACH 6–5, https://doi.org/10.1029/2001JD000511, http://dx.doi.org/10.1029/2001JD000511, 2002.

Drosdowsky, W.: Variability of the Australian Summer Monsoon at Darwin: 1957–1992, Journal of Climate, 9, 85–96, https://doi.org/10.1175/1520-0442(1996)009<0085:VOTASM>2.0.CO;2, https://doi.org/10.1175/1520-0442(1996)009<0085:VOTASM>2.0.CO;2, 1996.

Evans, S., Marchand, R., and Ackerman, T.: Variability of the Australian Monsoon and Precipitation Trends at Darwin, Journal of Climate, 27, 8487–8500, https://doi.org/10.1175/JCLI-D-13-00422.1, https://doi.org/10.1175/JCLI-D-13-00422.1, 2014.

Gu, J.-Y., Ryzhkov, A., Zhang, P., Neilley, P., Knight, M., Wolf, B., and Lee, D.-I.: Polarimetric Attenuation Correction in Heavy Rain at C Band, Journal of Applied Meteorology and Climatology, 50, 39–58, https://doi.org/10.1175/2010JAMC2258.1, https://doi.org/10.1175/2010JAMC2258.1, 2011.

Hagos, S., Feng, Z., Landu, K., and Long, C. N.: Advection, moistening, and shallow-to-deep convection transitions during the initiation and propagation of Madden-Julian Oscillation, Journal of Advances in Modeling Earth Systems, 6, 2013.

Hagos, S., Feng, Z., Plant, R. S., Houze, R. A., and Xiao, H.: A Stochastic Framework for Modeling the Population Dynamics of Convective Clouds, Journal of Advances in Modeling Earth Systems, 10, 448–465, https://doi.org/10.1002/2017MS001214, https://agupubs.onlinelibrary.wiley.com/doi/abs/10.1002/2017MS001214, 2018.

Hamada, A. and Nishi, N.: Development of a Cloud-Top Height Estimation Method by Geostationary Satellite Split-Window Measurements Trained with CloudSat Data, Journal of Applied Meteorology and Climatology, 49, 2035–2049, https://doi.org/10.1175/2010JAMC2287.1, https://doi.org/10.1175/2010JAMC2287.1, 2010.

Helmus, J. and Collis, S.: The Python ARM Radar Toolkit (Py-ART), a Library for Working with Weather Radar Data in the Python Programming Language, Journal of Open Research Software, 4, https://doi.org/10.5334/jors.119, http://openresearchsoftware.metajnl.com/articles/10.5334/jors.119/, 2016.

Jensen, E. J., Kinne, S., and Toon, O. B.: Tropical cirrus cloud radiative forcing: Sensitivity studies, Geophysical Research Letters, 21, 2023–2026, https://doi.org/10.1029/94GL01358, http://dx.doi.org/10.1029/94GL01358, 1994.

Johnson, R. H., Rickenbach, T. M., Rutledge, S. A., Ciesielski, P. E., and Schubert, W. H.: Trimodal Characteristics of Tropical Convection, Journal of Climate, 12, 2397–2418, https://doi.org/10.1175/1520-0442(1999)012<2397:TCOTC>2.0.CO;2, https://doi.org/10.1175/1520-0442(1999)012<2397:TCOTC>2.0.CO;2, 1999.

Keenan, T., Glasson, K., Cummings, F., Bird, T. S., Keeler, J., and Lutz, J.: The BMRC/NCAR C-Band Polarimetric (C-POL) Radar System, Journal of Atmospheric and Oceanic Technology, 15, 871–886, https://doi.org/10.1175/1520-0426(1998)015<0871:TBNCBP>2.0.CO;2, https://doi.org/10.1175/1520-0426(1998)015<0871:TBNCBP>2.0.CO;2, 1998.

Keenan, T. D., Manton, M. J., Holland, G. J., and Morton, B. R.: The Island Thunderstorm Experiment (ITEX)—A Study of Tropical Thunderstorms in the Maritime Continent, Bulletin of the American Meteorological Society, 70, 152–159, https://doi.org/10.1175/1520-0477(1989)070<0152:TITESO>2.0.CO;2, https://doi.org/10.1175/1520-0477(1989)070<0152:TITESO>2.0.CO;2, 1989.

Kumar, V. V., Jakob, C., Protat, A., May, P. T., and Davies, L.: The four cumulus cloud modes and their progression during rainfall events: A C-band polarimetric radar perspective, Journal of Geophysical Research: Atmospheres, 118, 8375–8389, https://doi.org/10.1002/jgrd.50640, http://dx.doi.org/10.1002/jgrd.50640, 2013a.

Kumar, V. V., Protat, A., May, P. T., Jakob, C., Penide, G., Kumar, S., and Davies, L.: On the Effects of Large-Scale Environment and Surface Types on Convective Cloud Characteristics over Darwin, Australia, Monthly Weather Review, 141, 1358–1374, https://doi.org/10.1175/MWR-D-12-00160.1, https://doi.org/10.1175/MWR-D-12-00160.1, 2013b.

Kumar, V. V., Jakob, C., Protat, A., Williams, C. R., and May, P. T.: Mass-Flux Characteristics of Tropical Cumulus Clouds from Wind Profiler Observations at Darwin, Australia, Journal of the Atmospheric Sciences, 72, 1837–1855, https://doi.org/10.1175/JAS-D-14-0259.1, https://doi.org/10.1175/JAS-D-14-0259.1, 2015.

Madden, R. A. and Julian, P. R.: Detection of a 40–50 Day Oscillation in the Zonal Wind in the Tropical Pacific, Journal of the Atmospheric Sciences, 28, 702–708, https://doi.org/10.1175/1520-0469(1971)028<0702:DOADOI>2.0.CO;2, https://doi.org/10.1175/1520-0469(1971)028<0702:DOADOI>2.0.CO;2, 1971.

Masunaga, H. and Luo, Z. J.: Convective and large-scale mass flux profiles over tropical oceans determined from synergistic analysis of a suite of satellite observations, Journal of Geophysical Research: Atmospheres, 121, 7958–7974, https://doi.org/10.1002/2016JD024753, https://agupubs.onlinelibrary.wiley.com/doi/abs/10.1002/2016JD024753, 2016.

May, P. T. and Ballinger, A.: The Statistical Characteristics of Convective Cells in a Monsoon Regime (Darwin, Northern Australia), Monthly Weather Review, 135, 82–92, https://doi.org/10.1175/MWR3273.1, https://doi.org/10.1175/MWR3273.1, 2007.

May, P. T. and Rajopadhyaya, D. K.: Vertical Velocity Characteristics of Deep Convection over Darwin, Australia, Monthly Weather Review, 127, 1056–1071, https://doi.org/10.1175/1520-0493(1999)127<1056:VVCODC>2.0.CO;2, https://doi.org/10.1175/1520-0493(1999)127<1056:VVCODC>2.0.CO;2, 1999.

May, P. T., Long, C. N., and Protat, A.: The Diurnal Cycle of the Boundary Layer, Convection, Clouds, and Surface Radiation in a Coastal Monsoon Environment (Darwin, Australia), Journal of Climate, 25, 5309–5326, https://doi.org/10.1175/JCLI-D-11-00538.1, https://doi.org/10.1175/JCLI-D-11-00538.1, 2012.

Minnis, P., Sun-Mack, S., Young, D. F., Heck, P. W., Garber, D. P., Chen, Y., Spangenberg, D. A., Arduini, R. F., Trepte, Q. Z., Smith, W. L., Ayers, J. K., Gibson, S. C., Miller, W. F., Hong, G., Chakrapani, V., Takano, Y., Liou, K. N., Xie, Y., and Yang, P.: CERES Edition-2 Cloud Property Retrievals Using TRMM VIRS and Terra and Aqua MODIS Data 2014; Part I: Algorithms, IEEE Transactions on Geoscience and Remote Sensing, 49, 4374–4400, https://doi.org/10.1109/TGRS.2011.2144601, 2011.

Nesbitt, S. W. and Zipser, E. J.: The Diurnal Cycle of Rainfall and Convective Intensity according to Three Years of TRMM Measurements, Journal of Climate, 16, 1456–1475, https://doi.org/10.1175/1520-0442(2003)016<1456:TDCORA>2.0.CO;2, https://journals.ametsoc.org/doi/abs/10.1175/1520-0442%282003%29016%3C1456%3ATDCORA%3E2.0.CO%3B2, 2003.

Nesbitt, S. W., Cifelli, R., and Rutledge, S. A.: Storm Morphology and Rainfall Characteristics of TRMM Precipitation Features, Monthly Weather Review, 134, 2702–2721, https://doi.org/10.1175/MWR3200.1, https://doi.org/10.1175/MWR3200.1, 2006.

Ohkawara, N.: Multi-Functional Transport Satellite (mtsat), https://doi.org/10.1.1.4.8950, http://citeseerx.ist.psu.edu/viewdoc/download?doi=10.1.1.4.8950&rep=rep1&type=pdf, 2004.

Pope, M., Jakob, C., and Reeder, M. J.: Regimes of the North Australian Wet Season, Journal of Climate, 22, 6699–6715, https://doi.org/10.1175/2009JCLI3057.1, https://doi.org/10.1175/2009JCLI3057.1, 2009a.

Pope, M., Jakob, C., and Reeder, M. J.: Objective Classification of Tropical Mesoscale Convective Systems, Journal of Climate, 22, 5797–5808, https://doi.org/10.1175/2009JCLI2777.1, https://doi.org/10.1175/2009JCLI2777.1, 2009b.

Rauniyar, S. and Walsh, K.: Spatial and temporal variations in rainfall over Darwin and its vicinity during different large-scale environments, Climate Dynamics, 46, https://doi.org/10.1007/s00382-015-2606-1, https://doi.org/10.1007/s00382-015-2606-1, 2016.

Rowe, A. K. and Houze, R. A.: Microphysical characteristics of MJO convection over the Indian Ocean during DYNAMO, Journal of Geophysical Research: Atmospheres, 119, 2014.

Rutledge, S. A., Williams, E. R., and Keenan, T. D.: The Down Under Doppler and Electricity Experiment (DUNDEE): Overview and Preliminary Results, Bulletin of the American Meteorological Society, 73, 3–16, https://doi.org/10.1175/1520-0477(1992)073<0003:TDUDAE>2.0.CO;2, https://doi.org/10.1175/1520-0477(1992)073<0003:TDUDAE>2.0.CO;2, 1992.

Steiner, M., Jr., R. A. H., and Yuter, S. E.: Climatological Characterization of Three-Dimensional Storm Structure from Operational Radar and Rain Gauge Data, Journal of Applied Meteorology, 34, 1978–2007, https://doi.org/10.1175/1520-0450(1995)034<1978:CCOTDS>2.0.CO;2, https://doi.org/10.1175/1520-0450(1995)034<1978:CCOTDS>2.0.CO;2, 1995.

Varble, A., Zipser, E. J., Fridlind, A. M., Zhu, P., Ackerman, A. S., Chaboureau, J.-P., Fan, J., Hill, A., Shipway, B., and Williams, C.: Evaluation of cloud-resolving and limited area model intercomparison simulations using TWP-ICE observations: 2. Precipitation microphysics, Journal of Geophysical Research: Atmospheres, 119, 13,919–13,945, https://doi.org/10.1002/2013JD021372, http://dx.doi.org/10.1002/2013JD021372, 2013JD021372, 2014.

Virts, K. S. and Houze, R. A.: Variation of Lightning and Convective Rain Fraction in Mesoscale Convective Systems of the MJO, Journal of the Atmospheric Sciences, 72, 1932–1944, https://doi.org/10.1175/JAS-D-14-0201.1, https://doi.org/10.1175/JAS-D-14-0201.1, 2015.

Wheeler, M. C. and Hendon, H. H.: An All-Season Real-Time Multivariate MJO Index: Development of an Index for Monitoring and Prediction, Monthly Weather Review, 132, 1917–1932, https://doi.org/10.1175/1520-0493(2004)132<1917:AARMMI>2.0.CO;2, https://doi.org/10.1175/1520-0493(2004)132<1917:AARMMI>2.0.CO;2, 2004.

Williams, E. R., Geotis, S. G., Renno, N., Rutledge, S. A., Rasmussen, E., and Rickenbach, T.: A Radar and Electrical Study of Tropical "Hot Towers", Journal of the Atmospheric Sciences, 49, 1386–1395, https://doi.org/10.1175/1520-0469(1992)049<1386:ARAESO>2.0.CO;2, https://doi.org/10.1175/1520-0469(1992)049<1386:ARAESO>2.0.CO;2, 1992.

Table 1. The average number of MCSes in the radar domain per scan identified using the criteria of (**?**) for the given MJO and monsoonal conditions.

Time of day	Break	Monsoon	MJO away from Australia	MJO over Australia
Total	0.17	0.30	0.14	0.24
Day	0.16	0.34	0.13	0.22
Night	0.18	0.26	0.14	0.24

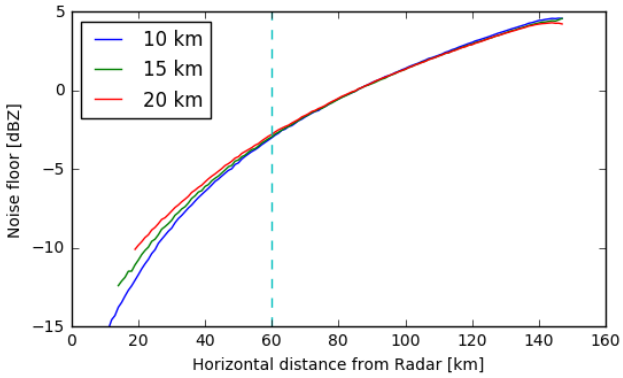

Figure 1. Minimum detectable signal of CPOL as a function of horizontal distance from CPOL for 3 vertical levels.

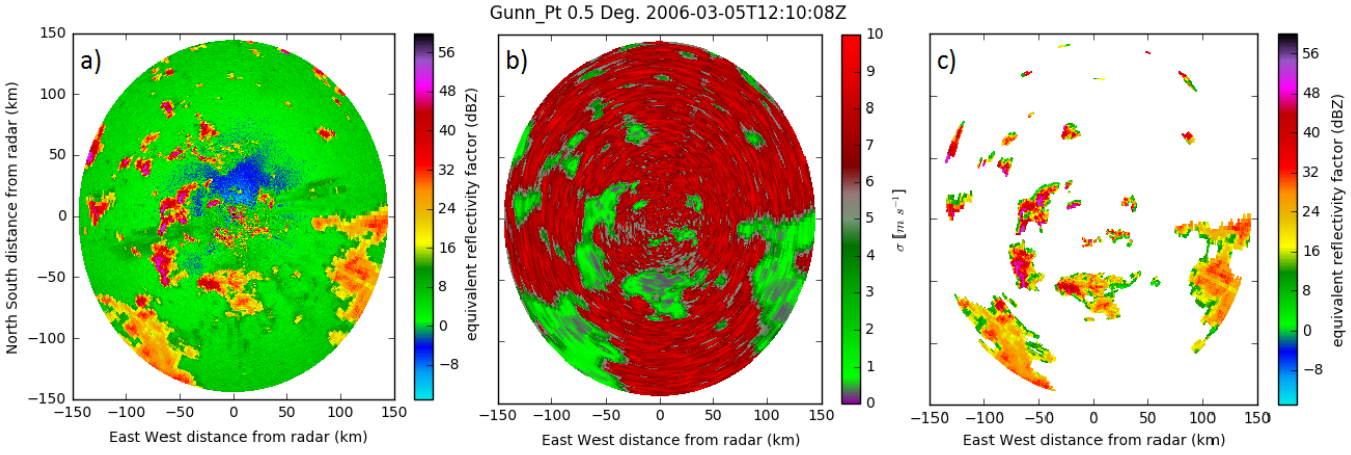

Figure 2. (a) Example Z (a) and (b) σ field for a PPI scan from CPOL on 05 March 2006. (c) Z after masking gates with $\sigma > 3$

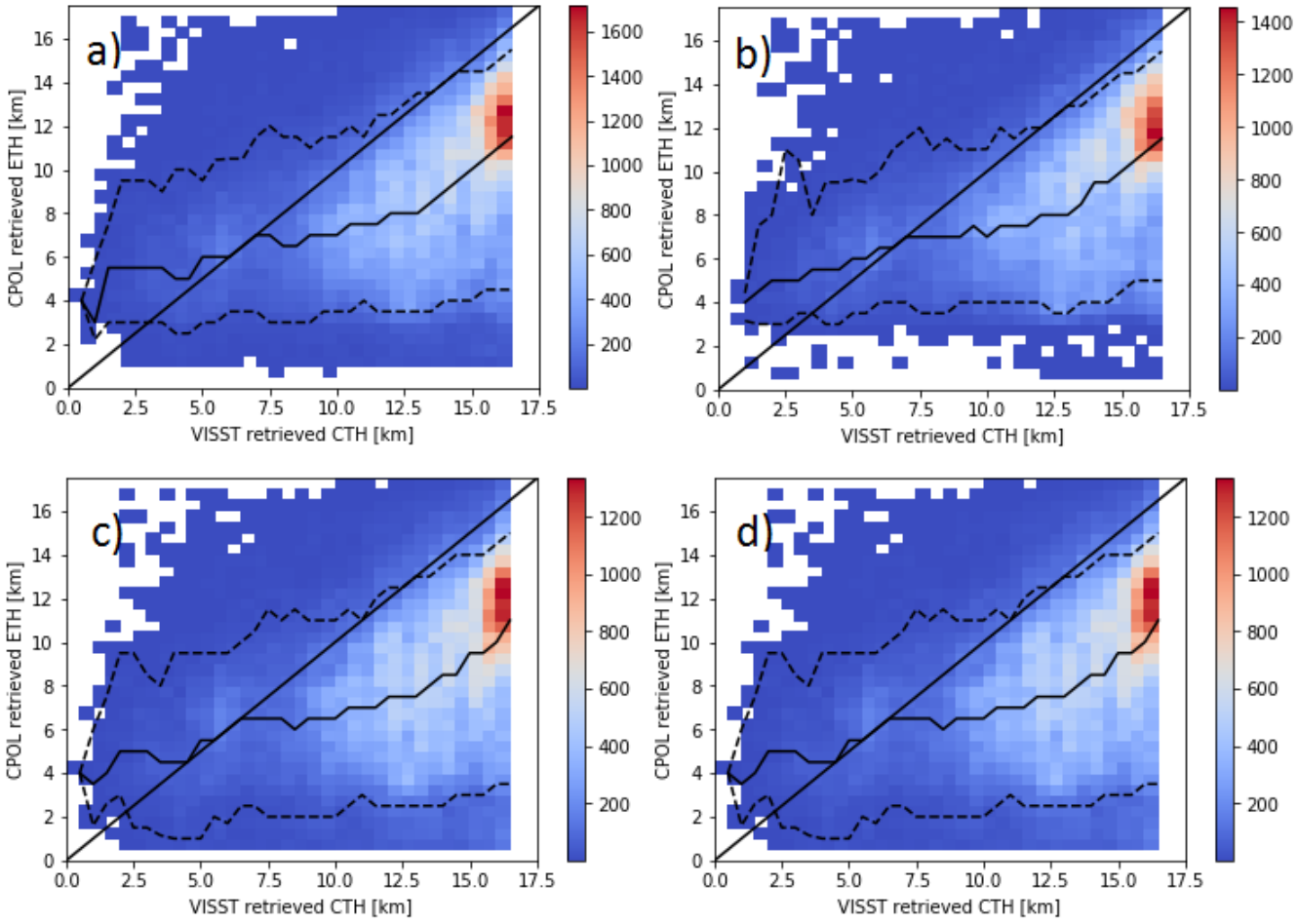

Figure 3. (a) ETH from CPOL retrieved using a Z threshold of 5 dBZ and (b) using a σ threshold of 2 $m\ s^{-1}$. (c) using a σ threshold of 3 $m\ s^{-1}$ and (d) 4 $m\ s^{-1}$. The dashed lines represent the 5th and 95th percentiles of CPOL ETH, while the solid line represents the median of the CPOL ETH. The shading represents the number of occurrences.

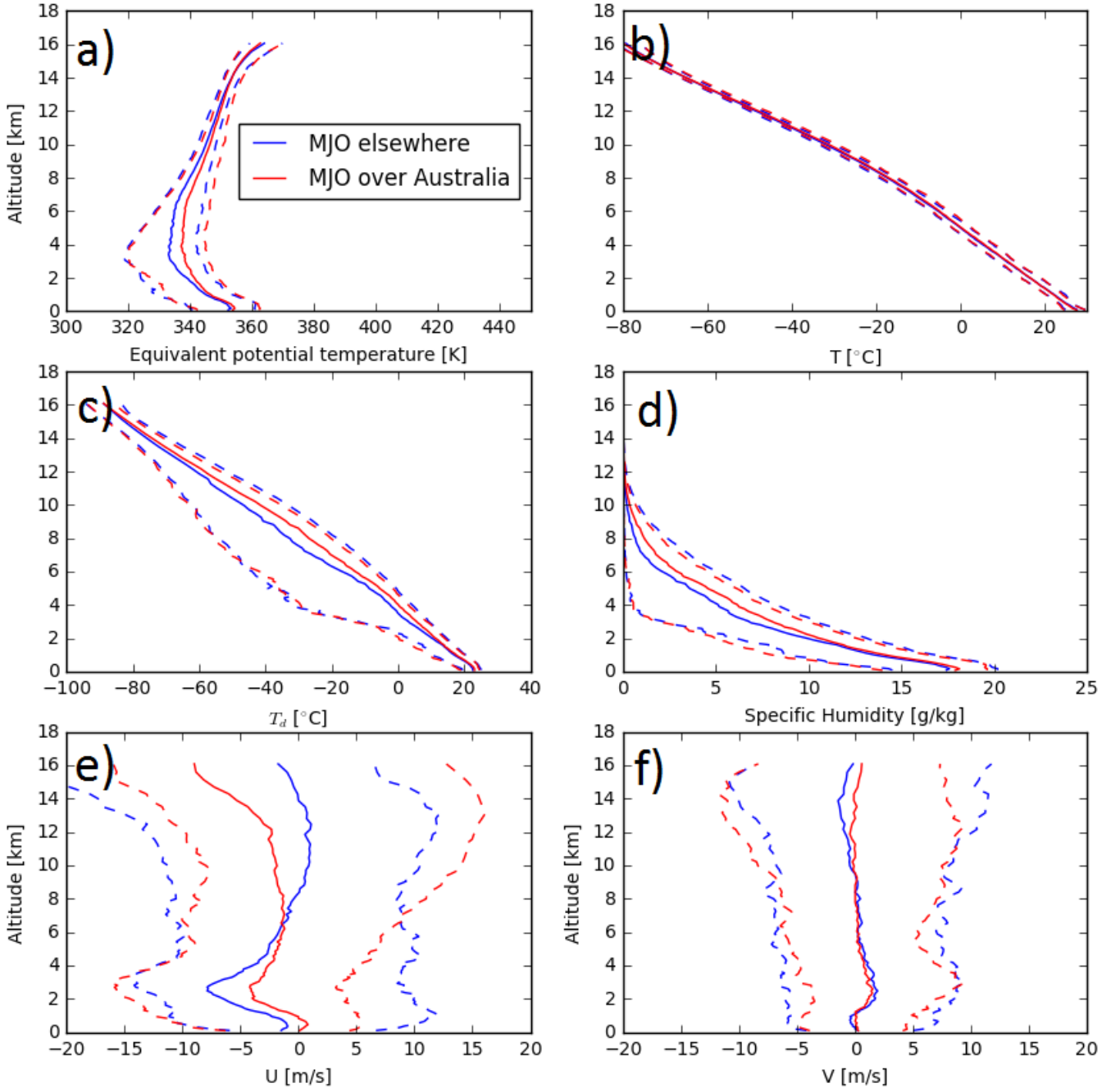

Figure 4. Mean ~~vertical profiles~~ (solid line) and 5th/95th percentiles (dashed lines) of (a) equivalent potential temperature, (b) temperature ~~and~~ , (c) dew point, (~~e~~d) specific humidity, (e) zonal wind and (~~d~~f) ~~mean~~ meridional wind as a function of height from 949 rawinsonde observations during break conditions.

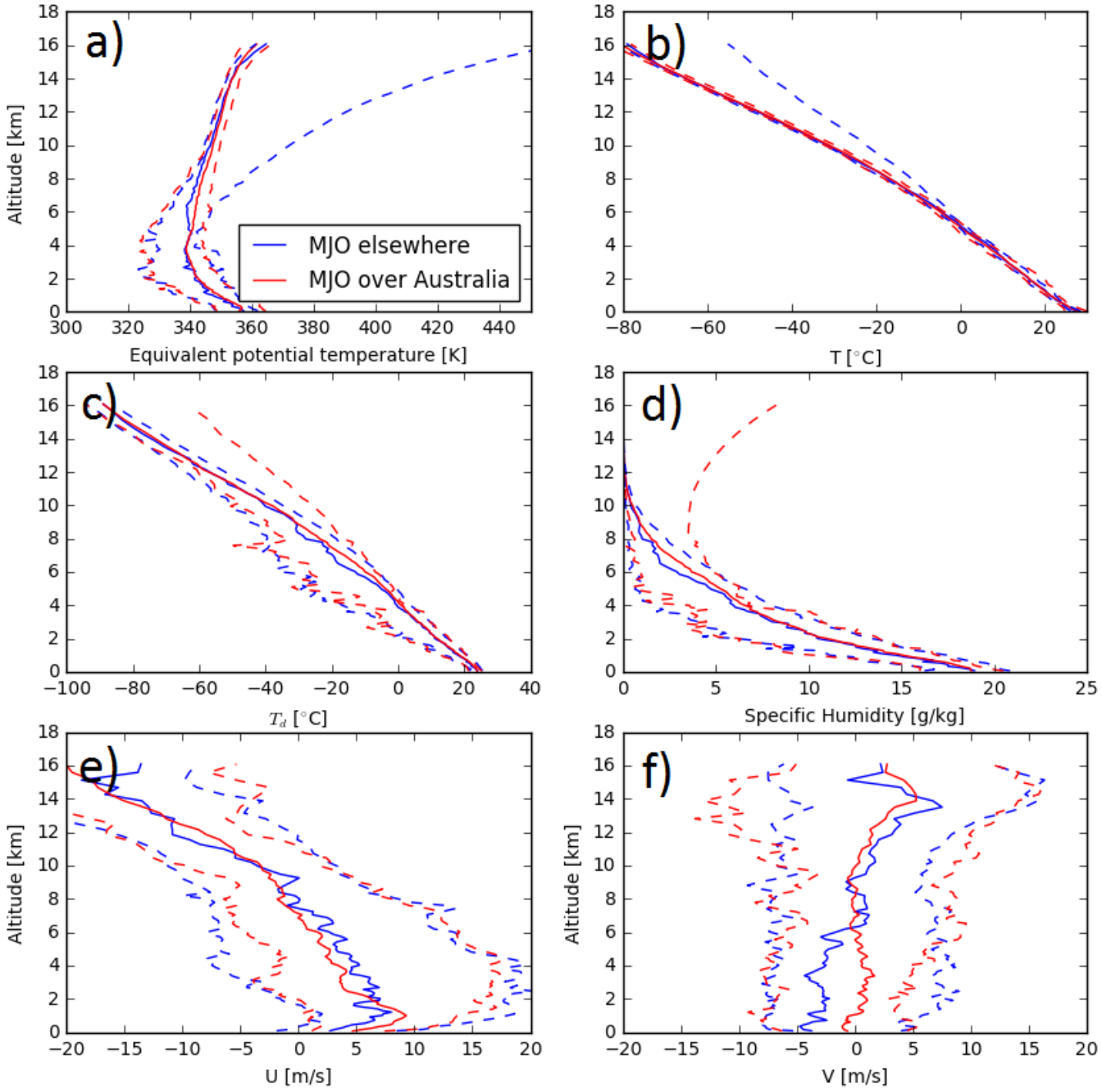

Figure 5. As Figure 4, but from 97 soundings taken during active monsoon conditions.

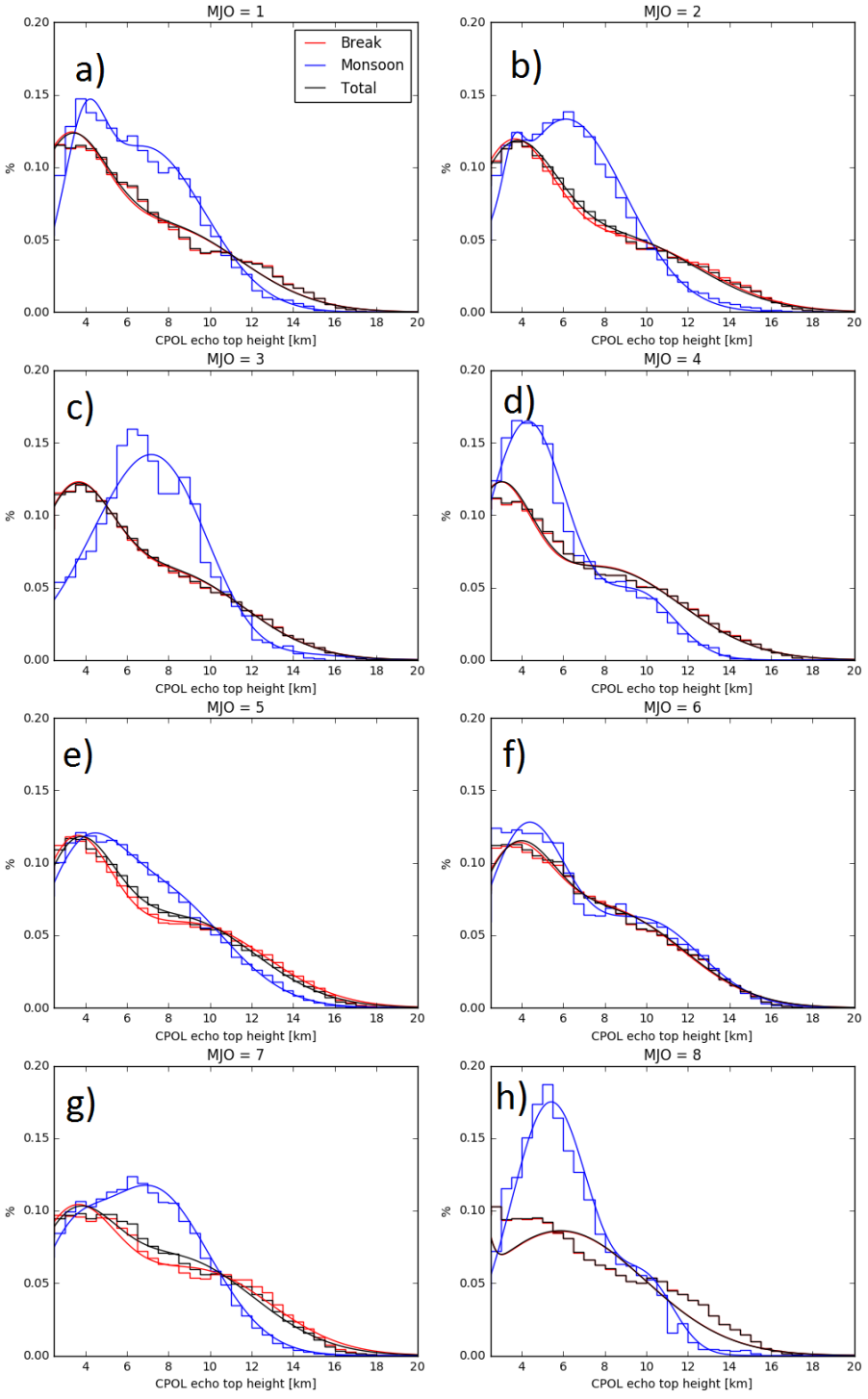

Figure 6. Normalized frequency distribution of ETHs in convective regions as a function of MJO index for break and monsoon conditions. Panels (a-h) each represent a different MJO index. Solid lines represent medians of modes derived from the fit of the bimodal Gaussian p.d.f. to the normalized frequency distribution.

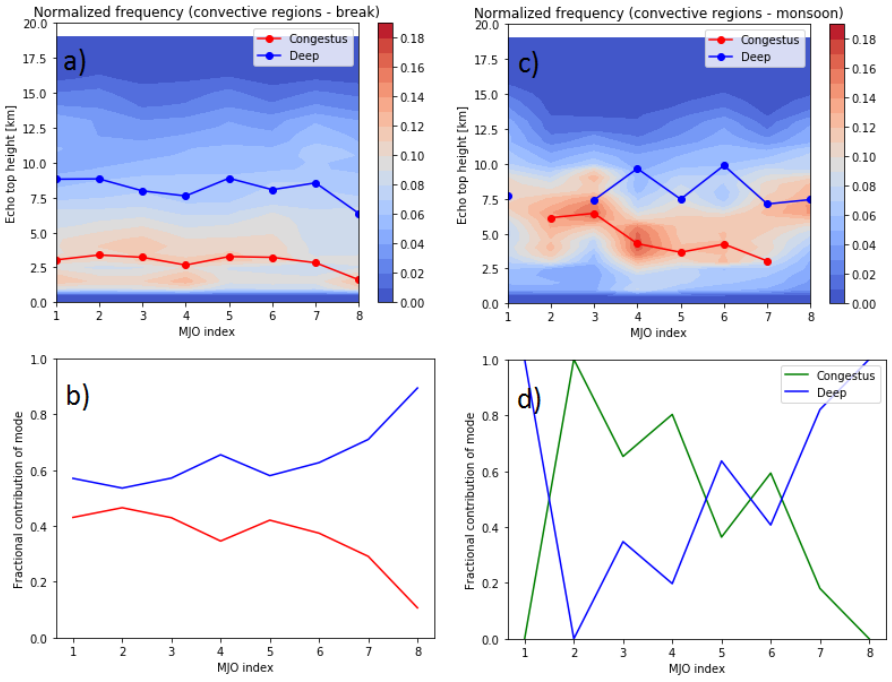

Figure 7. (a) ~~p.d.f.s~~ Normalized frequency distribution of ETHs in convective regions for given MJO ~~indices~~ indicies in break conditions. The color shading represents the normalized frequency. The red line is ~~μ_1~~ the location of the congestus mode and the blue line is ~~μ_2~~ the location of the deep convective mode. (b) Fractional contribution of each mode ~~(A (red line), 1-A (blue line))~~ to ~~p.d.f.s~~ normalized frequency distributions in (a). (c,d) as (a,b) but for monsoon conditions.

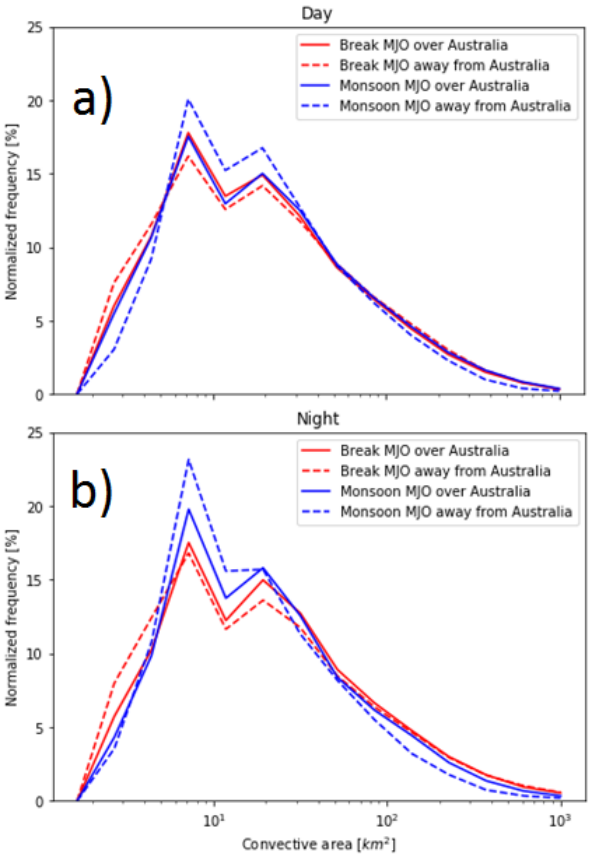

Figure 8. (a) Normalized frequency distribution of convective areas during the day (600 to 1900 local time). Each curve represents the large scale forcing specified in the legend. (b) as (a) but for night time.

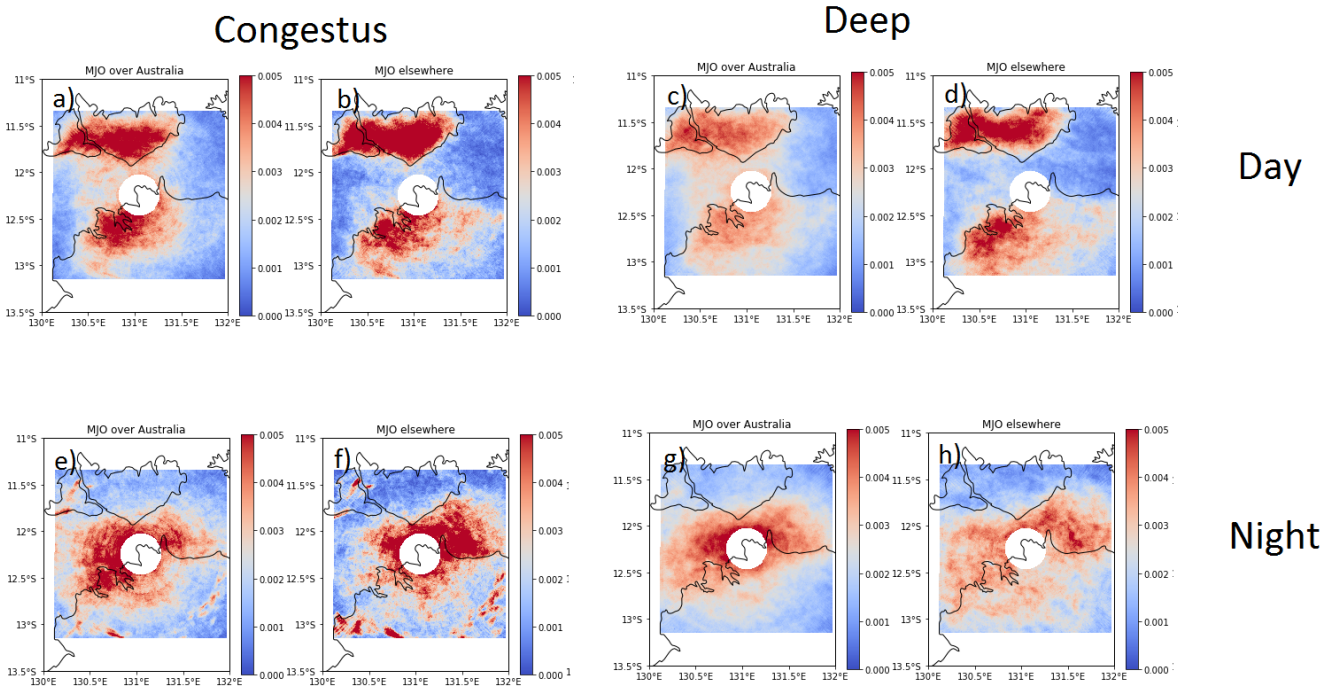

Figure 9. The normalized frequency of occurrence of ETHs < 7 km in MJO active (a) and ~~> 7 km for given phase of the~~ (b) MJO inactive conditions during the day (~~21~~ 600 to ~~10 UTC~~1900 local)~~and night~~ . (~~10~~ c,d) as (a,b) but for ETHs > 7 km. (e,f) as (a,b), but at night 1900 to ~~21 UTC~~600 local). (g,h) as (e,f), but for ETHs > 7 km. The histograms in Fig. 9 were taken during break conditions

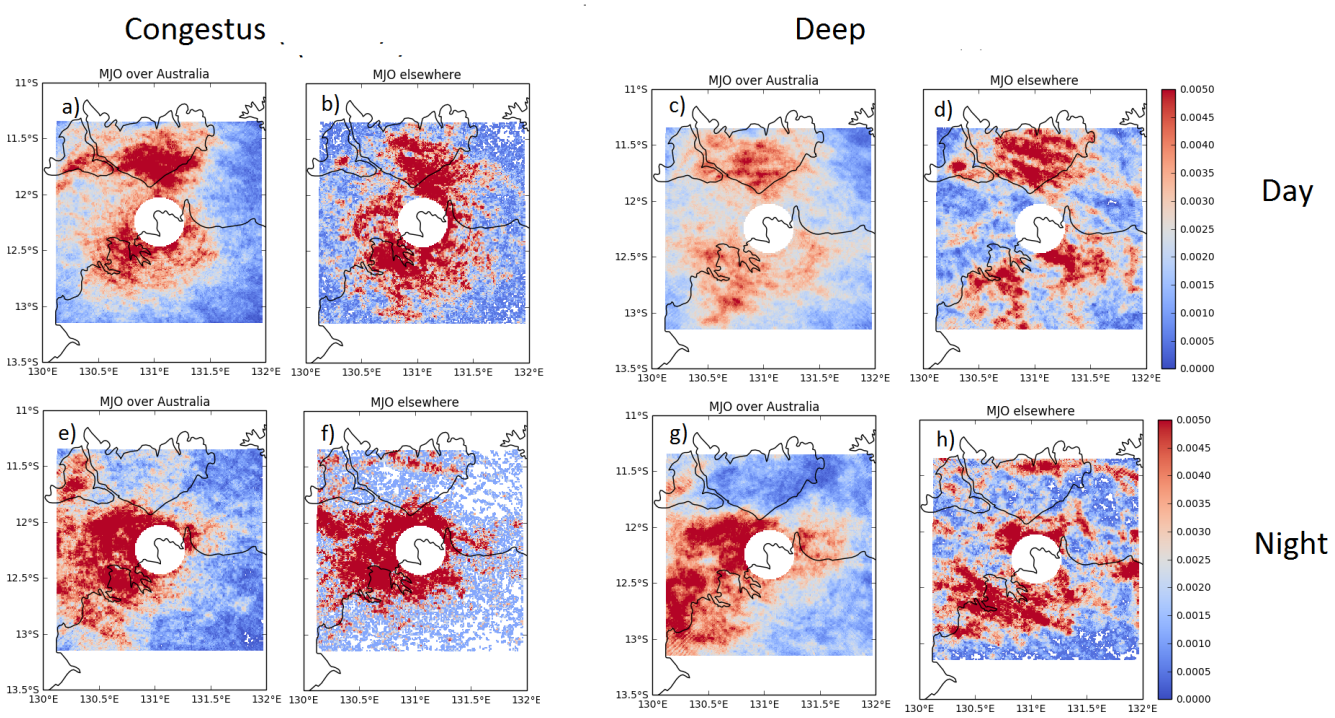

Figure 10. As Fig. ~~??~~9, but for active monsoon conditions.

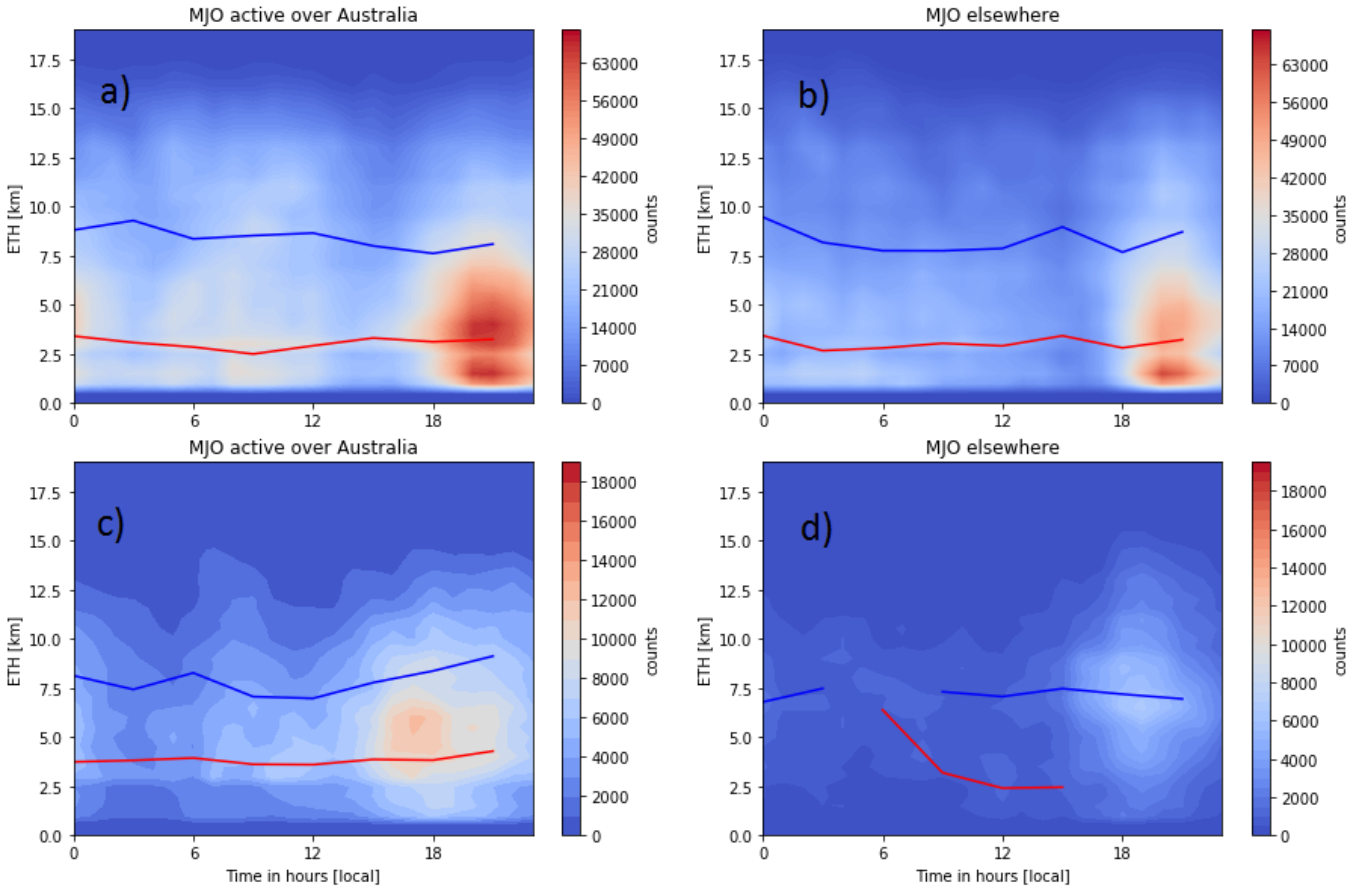

~~As Figure ??, but~~ during active monsoon conditions.

~~As Figure ??, but~~ during active monsoon conditions.

Figure 11. (a) Frequency distribution of occurrence of ETHs in convective regions as a function of time in break conditions when the MJO is active over Australia. Red line indicates peak of cumulus congestus mode, blue line indicates peak of deep mode of convection. (b) ~~The contribution of the cumulus congestus mode A and deep mode 1-A to the p.d.f of ETH~~ as (a) but for ~~the given hour. Shaded region indicates~~ when ~~it~~ the MJO is ~~night~~ inactive over ~~Darwin.~~ Australia (c,d) as (a,b) but ~~for when the active phase of the MJO is away from Darwin. As Figure ??, but~~ during active monsoon conditions.